

# A large population of metal-rich, compact, intergalactic C IV absorbers — Evidence for poor small-scale metal mixing<sup>\*</sup>

Joop Schaye<sup>1</sup>†, Robert F. Carswell<sup>2</sup>, Tae-Sun Kim<sup>3</sup>

<sup>1</sup> *Leiden Observatory, Leiden University, P.O. Box 9513, 2300 RA Leiden, The Netherlands*

<sup>2</sup> *Institute of Astronomy, Madingley Road, Cambridge CB3 0HA, U.K.*

<sup>3</sup> *Astrophysikalisches Institut Potsdam, An der Sternwarte 16, D-14482 Potsdam, Germany.*

12 June 2018

## ABSTRACT

We carried out a survey for high-metallicity C IV absorbers at redshift  $z \approx 2.3$  in 9 high-quality quasar spectra. Using a novel analysis technique, based on detections of C IV lines and automatically determined upper limits on the column densities of H I, C III, N V, and O VI, we find a large ( $dN/dz > 7$ ) population of photo-ionized, compact ( $R \sim 10^2$  pc), metal-rich ( $Z \gtrsim Z_{\odot}$ ) C IV clouds with moderate densities ( $n_{\text{H}} \sim 10^{-3.5} \text{ cm}^{-3}$ ), properties that we show are robust with respect to uncertainties in the ionization model. In particular, local sources of ionizing radiation, overabundance of oxygen, departures from ionization equilibrium, and collisional ionization would all imply more compact clouds. The clouds are too small to be self-gravitating and pressure confinement is only consistent under special conditions. We argue that the clouds are, in any case, likely to be short-lived and we demonstrate that this implies that the clouds could easily have been responsible for the transport of all metals that end up in the intergalactic medium (IGM). When metal-rich clouds reach pressure equilibrium with the general, photo-ionized IGM, the heavy elements will still be concentrated in small high-metallicity patches, but they will look like ordinary, low-metallicity absorbers. We conclude that intergalactic metals are poorly mixed on small scales and that nearly all of the IGM, and thus the universe, may therefore be of primordial composition.

**Key words:** cosmology: miscellaneous – galaxies: formation – intergalactic medium – quasars: absorption lines

## 1 INTRODUCTION

There is strong observational evidence that correlated supernova explosions drive gas flows into the halos of galaxies and into the intergalactic medium (IGM) through galactic fountain activity and massive superwinds (e.g., Veilleux et al. 2005). If the energy powering the outflows originates in supernovae, one would expect the outflowing gas to be highly enriched (e.g., Mac Low & Ferrara 1999). Indeed, X-ray observations of a starbursting dwarf galaxy indicate that nearly all the metals injected by the starburst are contained in a superwind (Martin, Kobulnicky, & Heckman 2002).

The outflowing gas will sweep up shells of gas, which may fragment due to hydrodynamical and thermal insta-

bilities and mix with the hot wind. Eventually the wind cools and the outflow decelerates. The shell fragments expand as the (ram) pressure drops, unless they become self-gravitating. The metals carried by the outflow will either rain back onto the galaxy or get mixed into the IGM, although this mixing could remain incomplete (e.g., Dedikov & Shchekinov 2004).

Careful studies of high-quality quasar absorption spectra have recently produced a wealth of information regarding the distribution of heavy elements in the high-redshift IGM. The abundance of carbon is found to be far below solar ( $[C/H] \approx -3$  at ten times the mean density and  $z = 3$ ; Schaye et al. 2003, hereafter S03; Simcoe et al. 2004) but with a large scatter ( $\sigma([C/H]) \approx 0.7$ , S03; Simcoe et al. 2004), to increase with density (S03), to be lower than that of oxygen (Telfer et al. 2002) and silicon (Aguirre et al. 2004), and to depend on the proximity to galaxies (e.g., Adelberger et al. 2003, 2005; Pieri et al. 2006). It is often not mentioned

<sup>\*</sup> Based on public data obtained from the ESO archive of observations from the UVES spectrograph at the VLT, Paranal, Chile.  
<sup>†</sup> E-mail: schaye@strw.leidenuniv.nl

that these measurements implicitly smooth over the scales associated with typical HI Ly $\alpha$  absorbers,  $R \lesssim 10^2$  kpc depending on the density (see Schaye & Aguirre 2005 and S03 for discussions). On smaller scales the distribution of metals is essentially unknown.

If the heavy elements that end up in the IGM were initially concentrated in gas clouds with very high metallicities, then what about the intermediate phase? Where are the high-metallicity, intergalactic gas clouds? Observing this phase is very important because it will give us valuable information regarding the physics of galactic winds, a key ingredient of theories of galaxy formation, and the enrichment of the IGM.

There are various strategies to look for high-metallicity gas flows from galaxies. Perhaps the most obvious strategy is to look for blueshifted absorption in the spectra of starburst galaxies. Such studies have provided unambiguous evidence for outflows containing heavy elements (e.g., Heckman et al. 2000; Pettini et al. 1998), but the faintness of the galaxies makes it very difficult to obtain spectra with sufficient resolution to resolve the substructure of the lines, let alone measure the corresponding metallicities. Another problem is that it is unclear how close to the galaxy the absorbing material is and therefore whether it can be considered extragalactic.

Some of these problems can be circumvented by searching for metal-line absorption along sight lines to bright background quasars which pass close to galaxies known to be driving winds (e.g., Norman et al. 1996, Chen et al. 2001; Adelberger et al. 2003; Simcoe et al. 2006; Stocke et al. 2006). The drawback here is that only a very small fraction of observed galaxies are close to a background source that is sufficiently bright to do high-resolution spectroscopy. Ultraviolet metal line *emission*, which could remain observable above the background out to  $\sim 10^2$  kpc from galaxies (Furlanetto et al. 2004), is another promising tool, particularly because it would provide spatial information that cannot be obtained from single line-of-sight absorption spectra.

Highly enriched gas clouds are regularly found in surveys for quasar absorption lines, for a wide range of redshifts and HI column densities (e.g., Carswell, Schaye, & Kim 2002; Tripp et al. 2002, 2006; Rigby et al. 2002; Charlton et al. 2003; Bergeron & Herbert-Fort 2005; Aracil et al. 2006; Simcoe et al. 2006; Péroux et al. 2006; Prochaska et al. 2006; Keeney et al. 2006). In their survey of O VI absorption at  $z \sim 2.5$ , Carswell et al. (2002) found one unusual system that showed absorption by HI, CIV, NV, and O VI. The system is unusual in that the HI absorption was very weak compared to the metal lines, and that it showed clear NV absorption. If the system is photoionized, then it must be very compact ( $\sim 10^2$  pc). Carswell et al. (2002) were able to show that regardless of the ionization mechanism, the metallicity must be high ( $\gtrsim$  solar) and the system cannot be self-gravitating, unless the gas fraction is negligible. Similar clouds have later been found in the survey for O VI absorption by Bergeron & Herbert-Fort (2005), whereas the survey for strong O VI absorption by Simcoe et al. (2006) turned up higher density analogs.

Here we describe a survey for high-metallicity CIV clouds in 9 high-quality quasar spectra at  $z \approx 2.3$ . We introduce a novel analysis technique, combining measurements of CIV column densities with automatically determined up-

per limits on the column densities of HI, CIV, NV, O VI, and Si IV. Our reliance on blindly measured upper limits for all transitions other than CIV makes our analysis robust to uncertainties due to blending, contamination, noise, and the presence of multiple phases. We find a large number of high-metallicity ( $Z > 0.1Z_{\odot}$ ) clouds and demonstrate that they are photo-ionized, moderately overdense, compact, and not gravitationally confined. In the second part of this paper we investigate the implications of the existence of this population, and other metal-rich populations found by others. We show that the clouds are probably short-lived, which implies that they could easily have been responsible for the transport of all the metals that end up in the IGM. Finally, we argue that it is likely that most intergalactic metals reside in small patches of high-metallicity gas, but that we generally cannot tell this observationally once the clouds have reached pressure equilibrium with their environments. This would mean that nearly all the gas in the universe is metal-free and that the generally accepted low IGM metallicities are only appropriate when averaged over large scales.

This paper is organized as follows. We begin with a brief description of the observations. Section 3 describes our analysis technique and the selection of the metal-rich sample. Results that are independent of the ionization model are described in §4, while §5 presents and discusses the method, results, and uncertainties of the ionization model. In §6 we compare our results with other observations and we investigate the implications for the nature and origin of the clouds, for the distribution of heavy elements, and for the interpretation of quasar absorption line studies. Finally, we provide a concise summary in §7. Given the length of the paper, we recommend reading the summary first.

All abundances are given by number relative to hydrogen, and solar abundances are taken to be the default values in CLOUDY96<sup>1</sup>:  $(C/H)_{\odot} = -3.61$ ,  $(N/H)_{\odot} = -4.07$ ,  $(O/H)_{\odot} = -3.31$ , and  $(Si/H)_{\odot} = -4.46$ .

## 2 OBSERVATIONS

We analyzed a sample of 9 high-quality (6.6 km s<sup>-1</sup> velocity resolution (FWHM), signal-to-noise ratio > 40) absorption spectra of  $2.1 \leq z \leq 3.3$  quasars taken with the UV-Visual Echelle Spectrograph (UVES; D’Odorico et al. 2000) on the Very Large Telescope (VLT). The quasars and their emission redshifts are listed in columns 1 and 2 of Table 1. The data reduction procedures were the same as those used by Kim et al. (2002).

We searched for all CIV systems between  $z_{\min} \leq z \leq z_{\max}$  irrespective of the presence of the associated HI. The minimum redshift  $z_{\min} \equiv \max(2.0, (1 + z_{\text{em}})1215.67/1548.20 - 1)$  was chosen to ensure that the corresponding O VI lines fall in the observed wavelength range and that CIV falls redwards of the quasar’s Ly $\alpha$  emission line (to prevent contamination by HI). To avoid proximity effects, a high redshift cutoff was imposed at  $z_{\max} \equiv z_{\text{em}} - (1 + z_{\text{em}})\Delta v/c$ , where  $\Delta v = \max(4000, 8\text{Mpc } H(z)/h)$  km s<sup>-1</sup> and  $H(z)$  is the Hubble

<sup>1</sup> See <http://www.nublado.org/>

<sup>2</sup> For HE0151–4326 a larger region was excluded to avoid broad, associated absorption lines.

parameter at redshift  $z$  extrapolated from its present value ( $H_0 \equiv 100h \text{ km s}^{-1} \text{ Mpc}^{-1}$ ) assuming  $(\Omega_m, \Omega_\Lambda) = (0.3, 0.7)$ . The search ranges and some information on the detected high-metallicity C IV systems are given in Table 1.

### 3 SELECTION OF HIGH-METALLICITY C IV ABSORBERS

We wish to select C IV lines that arise in gas with relatively high metallicity,  $Z > 0.1Z_\odot$ , and we wish to do this in a way that is robust with respect to problems due to line blending, noise, contamination, and uncertainties in the ionization models.

Our search for highly enriched, highly ionized gas clouds comprises the following main steps: (1) Identify all detectable C IV absorption lines which fall redwards of the quasar’s Ly $\alpha$  emission line and which have  $z_{\min} < z < z_{\max}$  ( $z_{\min}$  is chosen to ensure that O VI falls within the observed wavelength range and  $z_{\max}$  is chosen to avoid the region close to the quasar); (2) Decompose the C IV systems into Voigt profile components with parameters  $z$ ,  $N$  (column density), and  $b$  (line width); (3) For each component, determine conservative upper limits on the associated column densities of HI, NV, O VI, and other transitions of interest that fall within the observed wavelength range (e.g., C III and Si IV). We choose to work only with upper limits because it is in general impossible to measure reliable column densities for transitions that fall bluewards of the quasar’s Ly $\alpha$  emission line due to line blending (most important for HI) and the presence of contamination (important for C III, NV, and O VI); (4) Assuming photoionization by a given radiation field, select those components which must have a carbon abundance greater than 10% solar based on the measured lower limits on  $N_{\text{CIV}}/N_{\text{HI}}$  plus those on  $N_{\text{CIV}}/N_{\text{NV}}$  and/or  $N_{\text{CIV}}/N_{\text{OVI}}$  (the selection turns out to be nearly independent of the latter two measurements). In the following we will discuss the last three steps in more detail.

All detected C IV systems were decomposed into Voigt profile components using the VPFIT program described by Webb (1987) and Rauch et al. (1992) and updated by R.F. Carswell et al.<sup>3</sup>. The decomposition of any absorption system into Voigt profiles is generally not unique and may depend on the signal-to-noise ratio of the spectrum. However, we stress that the two processes that most complicate the decomposition of HI Ly $\alpha$  profiles, line blending and contamination, are much less important for C IV because the latter is a doublet, because we limit our search to the region redwards of the quasar’s Ly $\alpha$  emission line, and because C IV lines are much narrower and rarer than Ly $\alpha$  lines.

Because of the severe line blending and contamination in the Ly $\alpha$  and Ly $\beta$  forests, we do not attempt to measure the column densities associated with transitions that fall bluewards of the quasar’s Ly $\alpha$  emission line. Instead, we only consider robust upper limits on the column densities, a method which is conservative for our purposes. Note that this approach also circumvents problems due to both the possible multiphase nature of the absorbers and projection

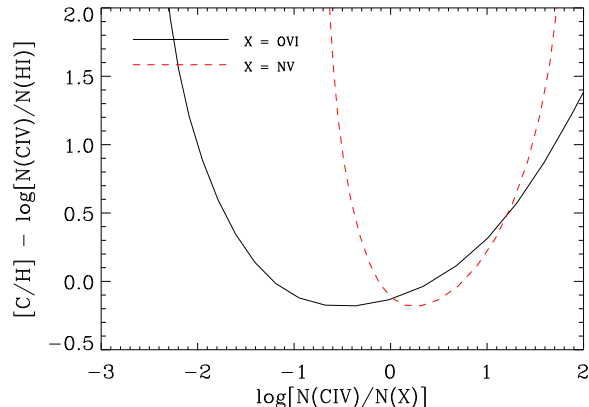


**Figure 1.** Metallicity as a function of the measured column density ratios. The C IV/HI column density ratio is assumed to be unity, the inferred metallicity is proportional to this ratio.

effects in velocity space (i.e., the redshift coincidence of absorption lines that arise in separate spatial locations). For example, if the absorption by HI at the redshift of the C IV absorber arises in different gas than the C IV absorption, then the HI column corresponding to the gas responsible for the C IV absorption will be lower than the upper limit we measure from the data.

We wrote a program to automatically compute upper limits on the associated column densities. The algorithm is fed a list containing the redshifts, Doppler parameters ( $b$ -values) and  $b$ -value error estimates for the C IV absorbers, determines the possible Doppler parameters for other elements assuming a range from pure turbulent to pure thermal broadening, and returns upper limits based on the spectrum, continuum and noise array. The algorithm is described in more detail in the Appendix.

We can write the abundance of carbon as

$$\begin{aligned} [\text{C}/\text{H}] &= \log\left(\frac{n_{\text{C}}}{n_{\text{CIV}}} \frac{n_{\text{CIV}}}{n_{\text{HI}}} \frac{n_{\text{HI}}}{n_{\text{H}}}\right) - \log\left(\frac{n_{\text{C}}}{n_{\text{H}}}\right)_{\odot} \quad (1) \\ &= \log\left(\frac{N_{\text{CIV}}}{N_{\text{HI}}}\right) - \log\left(\frac{n_{\text{CIV}}/n_{\text{C}}}{n_{\text{HI}}/n_{\text{H}}}\right) - \log\left(\frac{n_{\text{C}}}{n_{\text{H}}}\right)_{\odot} \quad (2) \end{aligned}$$

where the first term is an observable and the second term depends on the ionization balance.

Figure 1 shows how  $[\text{C}/\text{H}] - \log[N_{\text{CIV}}/N_{\text{HI}}]$  varies as a function of two observable proxies for the density,  $N_{\text{CIV}}/N_{\text{OVI}}$  (*solid*) and  $N_{\text{CIV}}/N_{\text{NV}}$  (*dashed*). As is the case for all ionization models presented in this work, the ionization balance was computed using the publicly available software package CLOUDY (version 96; see Ferland et al. 1998 and Ferland 2000 for details) and assuming ionization equilibrium. The gas was further assumed to be optically thin, to have solar relative abundances, to be at a temperature  $T = 10^4$  K, and to be exposed to the  $z = 2.3$  Haardt & Madau (2001) model of the UV/X-ray background from quasars and galaxies.

The minima in the curves correspond to the maximum  $n_{\text{CIV}}/n_{\text{HI}}$  ratio. Clearly, using this value will result in a robust lower limit on the metallicity. If the  $x$ -value (C IV/N V or C IV/O VI) is known, then this extra information can be used to obtain tighter constraints on the metallicity. In

<sup>3</sup> See <http://www.ast.cam.ac.uk/~rfc/vpfit.html>.

**Table 1.** Observed quasars

QSO (1)	$z_{\text{em}}$ (2)	$z_{\text{min}}$ (3)	$z_{\text{max}}$ (4)	# sys. (5)	$z_{\text{abs}}$ (6)	[C/H] > -1		all CIV	
						# comp. (7)	$ \Delta v $ (km s <sup>-1</sup> ) (8)	# comp. (9)	$ \Delta v $ (km s <sup>-1</sup> ) (10)
Q0122-380	2.181	2.00	2.14	1	2.063	1	0	1	0
Pks0237-233	2.225	2.00	2.18	1	2.042	2	27	5	121
HE1122-1648	2.400	2.00	2.35	1	2.030	1	0	1	0
HE2217-2818	2.406	2.00	2.36	0	0				
Q0329-385	2.423	2.00	2.38	2	2.076, 2.352	1, 2	0, 10	1, 2	0, 10
HE1347-2457	2.534	2.00	2.49	1	2.116	1	0	3	69
HE0151-4326	2.740	2.00	2.52	2	2.417, 2.468	2, 2	346, 54	4, 3	373, 54
HE2347-4342	2.900	2.07	2.85	2	2.120, 2.275	1, 7	0, 201	2, 9	14, 445
Pks2126-158	3.266	2.36	3.21	2	2.394, 2.679	6, 2	699, 12	12, 4	718, 54

<sup>a</sup> Cols. (1) and (2) contain the quasar name and redshift. Cols. (3) and (4) contain the minimum and maximum redshifts searched. Col. (5) shows the number of CIV systems with at least one component with [C/H] > -1, while col. (6) gives the redshifts of these absorption systems. Col. (7) and (8) shows, for each system, the total number of absorption line components with [C/H] > -1 and their maximum velocity separation. Finally, cols. (9) and (10) show, for the same systems, the number of components and their maximum velocity separation when all detected CIV components are taken into account, irrespective of their inferred lower limits on [C/H].

our case, we only have lower limits on the  $x$ -values, which means we can improve the lower limit on the metallicity if the observed  $x$ -value falls to the right of the minimum of the curve. It turns out, however, that the vast majority of our data points fall to the left of the minima.

Figure 2 shows the measured lower limits<sup>4</sup> on  $N_{\text{CIV}}/N_{\text{HI}}$ , for all 219 detected CIV components, as a function of the lower limits on  $N_{\text{CIV}}/N_{\text{OVI}}$  (*left*) and  $N_{\text{CIV}}/N_{\text{NV}}$  (*right*). The solid curves indicate the predicted ratios for a metallicity of 10% solar and a fixed temperature of (*from bottom-to-top*)  $\log T = 4.0, 4.8,$  and  $5.05$ , respectively. Density varies along these curves.

If our measurements of the OVI and NV column densities were detections rather than upper limits, and if we would know the temperature of the absorbers, then any point above the corresponding curve would have a metallicity greater than 10% solar. Since  $N_{\text{CIV}}/N_{\text{HI}}$  is proportional to metallicity, the vertical offset between the points and the curve can be used to determine the actual lower limit on the metallicity. However, since we only have a lower limit on the quantity plotted along the  $x$ -axes, we are allowed to shift all the points to the right. For points to the left of the maximum of the curve (which corresponds to the minimum of the curve plotted in Fig. 1), this would result in a decreased lower limit on the metallicity. On the other hand, if a point lies above the maximum of the curve, then shifting to the right will increase the lower limit on the metallicity. Taking into account the fact that  $x$ -value (a proxy for the density or ionization parameter) is only constrained from below, we see that only the points that fall above the dashed curve (which coincides with the  $\log T = 4.0$  solid curve beyond its peak) are constrained to have metallicities greater than 10% solar.

As we mentioned before, the peak in the curve cor-

responds to the density (ionization parameter) for which  $n_{\text{CIV}}/n_{\text{HI}}$  is maximum. For temperatures around  $10^4$  K collisional ionization is unimportant and this ratio is insensitive to the temperature (see, e.g., fig. 3 of S03). From figure 2 we can see that even for  $\log T = 4.8$  the maximum is nearly identical. For temperatures somewhat higher than this, collisional ionization results in a slightly higher peak value for the ratio  $n_{\text{CIV}}/n_{\text{HI}}$ . We find that the temperature has to differ from  $\log T = 5.05$  by less than about 0.2 dex for the peak to exceed that obtained when photo-ionization dominates, and even then the peak value is never boosted by more than a factor 5. Because of this relatively small difference and because, as we shall show later, such high temperatures are not favored by the data, we used the  $\log T = 4.0$  curve (dashed curve in Fig. 2) to select CIV components with [C/H] > -1.

For the selection of metal-rich clouds, the ratios  $N(\text{CIV})/N(\text{OVI})$  and  $N(\text{CIV})/N(\text{NV})$  only provide extra information for data points that fall above the curve, but below and to the right of its peak. In our case this is true for only 2 of the 28 clouds in our high-metallicity sample<sup>5</sup>. Not coincidentally, these are also the only two clouds for which only one of these two column density ratios results in the selection of the cloud. Thus, our sample would have been nearly identical if we had ignored our upper limits on  $N_{\text{OVI}}$  and  $N_{\text{NV}}$ .

The median lower limit on the metallicity for the sample of all 219 detected CIV components is [C/H] > -2.5. This value should not be interpreted as a lower limit on the median carbon abundance of the IGM, since we have ignored the many HI absorbers for which CIV was not detected.

Note that due to the conservative nature of our measurements and assumptions, our sample of high-metallicity CIV components may be highly incomplete. That is, had we been able to measure accurate column densities for HI,

<sup>4</sup> All limits on column density ratios involving CIV take the error on  $N_{\text{CIV}}$  into account.

<sup>5</sup> The two clouds are the ones at  $z = 2.119806$  in HE2347-4342 and at  $z = 2.393862$  in Pks2126-158

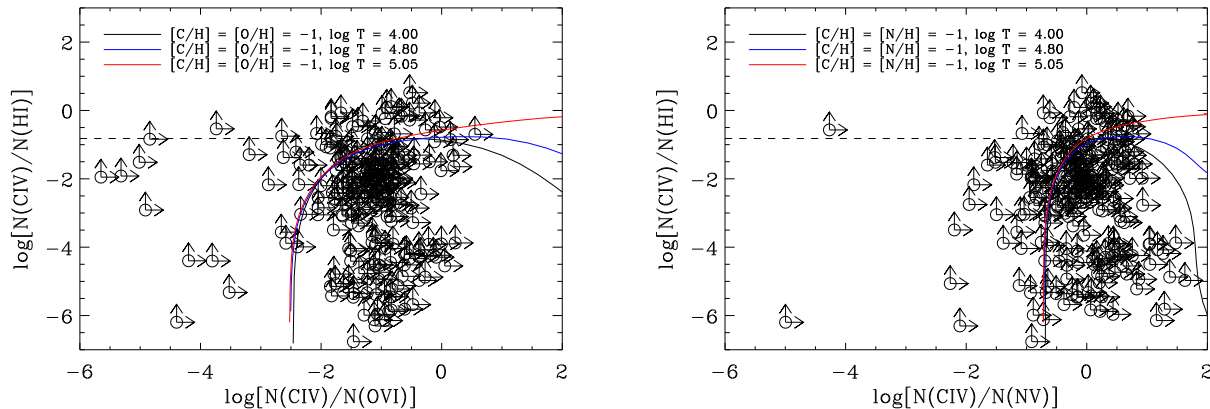


**Figure 2.** Data points indicate measured  $1\sigma$  lower limits on the C IV/H I column density ratio as a function of the  $1\sigma$  lower limits on the column density ratios C IV/O VI (*left*) and C IV/N V (*right*). From bottom-to-top the solid curves show the predicted ratio for a metallicity of 10% solar and temperatures of  $\log[T(\text{K})] = 4.00, 4.80,$  and  $5.05$ , respectively. The latter value corresponds roughly to the maximum C IV/H I ratio. Curves exceed the dashed line only for temperature within a factor of about two from this value. All points that are above at least one of the dashed curves (which coincide with the lowest solid curves to the right of their peaks) were selected as high-metallicity clouds.

N V, and O VI, then we might have found many more C IV components with  $[C/H] > -1$ .

#### 4 DIRECT OBSERVABLES

Our search of 9 quasar spectra resulted in a sample of 12 C IV systems which contain at least one component with  $[C/H] > -1$ . The total number of Voigt profile components with  $[C/H] > -1$ , which we will refer to as “high-metallicity clouds”, is 28. Columns 5–7 of Table 1 list, for each quasar, the number of high metallicity systems, their redshifts and their number of high-metallicity C IV components, respectively.

We define a system as a set of C IV components which span a redshift range  $\Delta z < 0.01$ . Of the 12 systems, 5 are consistent with a single-cloud structure, but this number reduces to 3 if all detected C IV components belonging to these systems are taken into account, rather than only those with inferred  $[C/H] > -1$  (the total number of detected C IV components is shown in col. 9). Column (8) of Table 1 contains, for each system, the velocity range spanned by the metal-rich clouds and column (10) shows the corresponding value if all C IV components are included. The maximum velocity difference between the metal-rich (all) C IV clouds is  $699 \text{ km s}^{-1}$  ( $718 \text{ km s}^{-1}$ ), while 8 (5) out of the 12 systems span less than  $30 \text{ km s}^{-1}$ .

The low rate of incidence of high-metallicity clouds ensures that the probability of a chance superposition on the velocity scales typical of the absorption systems ( $\Delta v \lesssim 10^2 \text{ km s}^{-1}$  which corresponds to  $\Delta z \lesssim 10^{-3}$ ) is negligibly small. Hence, there is little doubt that the components of a system are physically related.

The median and mean system redshifts are 2.28 and 2.25, respectively. The median redshift searched, i.e., the redshift below which half of the redshift path is located, is 2.24. The total redshift path searched is  $\Delta z = 4.05$ , which yields a rate of incidence  $dN/dz$  of  $3.0 \pm 0.9$  for  $[C/H] > -1$

systems and  $7 \pm 1$  for the individual  $[C/H] > -1$  clouds<sup>6</sup>. Because of the conservative nature of our selection criteria, these rates are likely to be underestimates.

Figures 9 – 22 show the spectral regions of interest for the 12  $[C/H] > -1$  absorption systems and Table 3 lists the Voigt profile fits to the C IV systems as well as the upper on the column densities of other ions.

Our spectral coverage enabled us to obtain  $1\sigma$  upper limits on the column densities of H I, N V, O VI, and Si IV for all the clouds. For 15 of the 28 clouds we were also able to measure upper limits on the C III column densities. Figure 3 shows the distributions of H I (*left, solid*), C IV (*left, dotted*), N V (*middle, solid*), O VI (*middle, dotted*), C III (*right, solid*), and Si IV (*right, dotted*) column densities of the high-metallicity clouds. The clouds in our sample span  $\log[N_{\text{CIV}} (\text{cm}^{-2})] = 11.8 - 13.9$  (median 13.0) and the median upper limits on the column densities of the other ions are 13.3 for H I, 12.9 for N V, 14.0 for O VI, 12.7 for C III, and 11.7 for Si IV.

It is interesting to compare these values to the ones obtained for the complete sample of C IV absorbers. The median C IV column for that sample is 0.5 dex lower than for the metal-rich sample, while the median upper limit on the column of H I is 1.2 dex higher. As expected from our selection criteria, the lower limits on the C IV/H I ratio are much higher for the metal-rich sample. Interestingly, the median upper limits on the N V and O VI column densities are only lower by 0.3 dex for the complete sample, which suggests that contamination and/or noise are important for these ions. For C III and Si IV the situation is even worse: the median upper limits on the column densities are lower for the metal-rich sample by 0.3 dex.

A worry for any quasar absorption line study, and particularly for those focusing on rare systems, is that some

<sup>6</sup> For  $(\Omega_m, \Omega_\Lambda) = (0.3, 0.7)$  and  $z = 2.3$  these rates correspond to number densities per unit absorption distance  $dN/dX$  of  $0.9 \pm 0.3$  and  $2.2 \pm 0.4$  for systems and clouds, respectively.

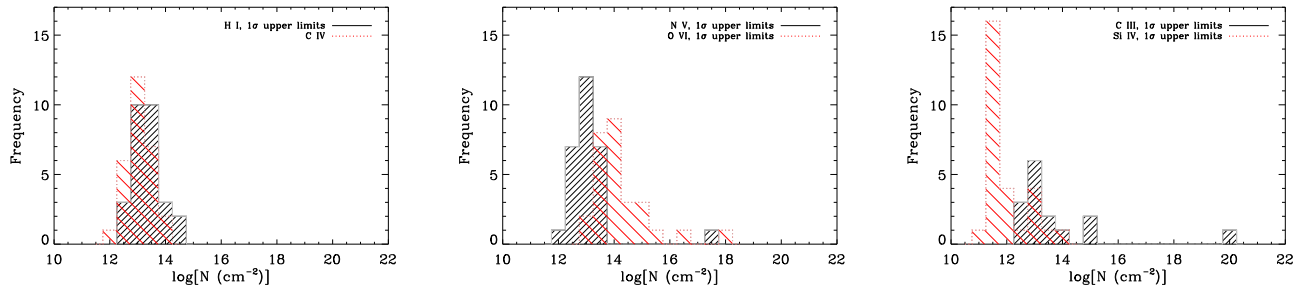


**Figure 3.** Histograms showing the column density distribution of HI (*left, solid*), CIV (*left, dotted*), NV (*middle, solid*), OVI (*middle, dotted*), CIII (*right, solid*), and SiIV (*right, dotted*) for the high-metallicity clouds listed in Table 3. Except for CIV, all column densities are  $1\sigma$  upper limits.

of the absorbers may be associated with (ejected by) the quasar rather than intervening. This, however, appears not to be the case for the systems studied here. Ejected systems tend to be very broad, show evidence for partial coverage of the emission source, and have a preference for redshifts close to that of the quasar (e.g., Hamann et al. 1997). The metal-rich clouds, on the other hand, are narrow (half of the CIV lines have  $b < 10 \text{ km s}^{-1}$ , see Table 3, col. 11), the doublet ratios show no evidence for partial coverage, and there is no evidence for an excess of absorbers near the redshift of the quasar: the median and mean values of the observable  $(z_{\text{abs}} - z_{\text{min}})/(z_{\text{max}} - z_{\text{min}})$  are 0.26 and 0.38, respectively, for the metal-rich systems. The Kolmogorov-Smirnov test gives a probability of 0.14 that the observable  $(z_{\text{abs}} - z_{\text{min}})/(z_{\text{max}} - z_{\text{min}})$  is drawn from a uniform distribution between 0 and 1. Hence, there is a mild tendency for the absorbers to reside in the low-redshift half of the redshift path searched. This can be explained as a result of the lower contamination of NV and HI, but is opposite to what one would expect for ejected systems. Most of the absorbers are, in fact, at large separations from the quasars: the median and mean velocity separations are both  $3.5 \times 10^4 \text{ km s}^{-1}$  and the velocity difference is greater than  $6.2 \times 10^3 \text{ km s}^{-1}$  in all cases. Thus, it is very likely that the metal-rich absorbers are intervening gas clouds.

Recently, Misawa et al. (2007) claimed that up to 17% of narrow absorption line CIV systems that are blueshifted by at least 5,000 km/s may show evidence for partial covering. If 17% of our systems were intrinsic, even though none of them show evidence for partial covering, our lower limit on the rate of incidence of high-metallicity CIV systems would have to be decreased by 17%, but this would not affect any of our conclusions.

As discussed in §2, regions close to the quasar were excluded to avoid proximity effects. If we had not excluded the regions between  $z_{\text{em}}$  and  $z_{\text{max}}$ , then we would have selected two more high-metallicity systems (both towards HE2347–4342). The rate of incidence of  $[C/H] > -1$  systems in the proximity zones is  $dN/dz = 3 \pm 2$ , which is consistent with the  $3.0 \pm 0.9$  found for the fiducial sample.

Column 3 of Table 2 lists for each metal-rich absorption system the velocity separation from the nearest HI Ly $\alpha$  line with  $N_{\text{HI}} > 10^{14.5} \text{ cm}^{-2}$ . For components in a complex the system with the smallest separation from the nearest high column density system has been chosen. The last column of the table gives the probability that the velocity separa-

**Table 2.** Relation to high  $N_{\text{HI}}$  absorbers

<i>a</i>			
QSO	$z_{\text{abs}}$	$\Delta v(N_{\text{HI}} > 10^{14.5})$ ( $\text{km s}^{-1}$ )	$P(< \Delta v)$
(1)	(2)	(3)	(4)
Q0122–380	2.063	1910	0.564
Pks0237–233	2.042	59	0.019
HE1122–1648	2.030	300	0.140
Q0329–385	2.076	6785	0.800
Q0329–385	2.352	1021	0.191
HE1347–2457	2.116	89	0.038
HE0151–4326	2.417	75	0.049
HE0151–4326	2.468	1406	0.542
HE2347–4342	2.120	2208	0.800
HE2347–4342	2.275	485	0.250
Pks2126–158	2.394	21	0.067
Pks2126–158	2.679	121	0.123

<sup>a</sup> Cols. (1) and (2) contain the quasar name and the absorber redshift, respectively. Col. (3) gives the velocity separation from the nearest Ly $\alpha$  absorber with  $N(\text{HI}) > 10^{14.5} \text{ cm}^{-2}$  and col. (4) gives the probability that the separation is this small or smaller if the metal-rich systems were randomly distributed.

tion is smaller than observed if the systems were positioned randomly between  $z_{\text{min}}$  and  $z_{\text{max}}$ . The data confirm the visual impression from figures 9 – 22: 6 absorption systems are probably associated with strong HI lines, 1 is possibly so ( $z = 2.352$  in Q0329 – 385,  $z = 2.275$  in HE2347 – 4342), and another 4 are not.

In summary, the  $[C/H] > -1$  systems (clouds) have a rate of incidence  $dN/dz > 3.0 \pm 0.9$  ( $7 \pm 1$ ) at a median redshift of  $z_{\text{abs}} = 2.3$ . They are a mixture of single cloud and multiple clouds systems. Some reside in the vicinity of  $N_{\text{HI}} > 10^{14.5} \text{ cm}^{-2}$ -systems, but many do not. The main difference with ordinary CIV systems is that the metal-rich clouds have higher CIV/HI ratios (by selection). Their distribution along the line of sight, their line widths, and their doublet ratios all suggest that they are intervening systems, rather than ejected by the quasar.

## 5 IONIZATION MODELING

In this section we will use ionization models to infer the physical characteristics of the high-metallicity clouds listed in Table 3.

Assuming photoionization and a fixed temperature, the column density ratios of the different ions depend only on the ambient radiation field, the gas density, and the relative abundances of the elements. In fact, for a fixed spectral shape of the UV/X-ray radiation, the ionization balance depends only on the ratio of the intensity to the gas density. It is therefore useful to parametrize the intensity by the “ionization parameter”, which is defined as,

$$U \equiv \frac{\Phi_{\text{H}}}{n_{\text{H}}c}, \quad (3)$$

where  $\Phi_{\text{H}}$  is the flux of hydrogen ionizing photons (i.e., photons per unit area and time),  $n_{\text{H}}$  is the total hydrogen number density, and  $c$  is the speed of light. For our fiducial radiation field, which we will take to be the Haardt & Madau (2001) model of the  $z = 2.3$  UV/X-ray background from quasars and galaxies, the ionization parameter is related to the gas density by

$$\log U \approx -4.70 - \log[n_{\text{H}}(\text{cm}^{-3})]. \quad (4)$$

Although we will generally quote densities rather than ionization parameters, it is important to keep in mind that only the ionization parameter is measurable from the observations presented here.

Since the O VI fraction peaks at a higher ionization parameter (i.e., a lower density for a fixed radiation field) than the N V fraction, which in turn peaks at a higher ionization parameter than the C IV fraction, we can use the two independent ratios that can be formed from these three column densities as indicators of the degree to which the systems are ionized. For example, if the relative abundances of the elements are approximately constant, more highly ionized clouds should have lower C IV/O VI and C IV/N V.

The solid curves in Figure 4 indicate the expected column density ratios for our fiducial radiation background, solar abundance ratios, and temperatures of, from right-to-left,  $\log T = 4.0, 5.1, 5.2,$  and  $5.3$ . For temperatures below  $10^5$  K the results are very close to those for  $10^4$  K. The dashed curve shows the results for pure collisional ionization equilibrium. Density varies along the solid curves (some values are indicated), while temperature varies along the dashed curve.

The left panel shows all detected C IV components while the right panel shows only the high-metallicity sample (in the left panel arrows have been suppressed for clarity). The points in the left panel roughly follow the trend  $\log[N_{\text{CIV}}/N_{\text{OVI}}] \propto \log[N_{\text{CIV}}/N_{\text{NV}}]$ , although with a large scatter, as would be expected if the measured upper limits on  $N_{\text{OVI}}$  and  $N_{\text{NV}}$  are dominated by contamination and are therefore independent of  $N_{\text{CIV}}$ . This suggests that the measurements are conservative lower limits, which may be significantly lower than the true values.

There are no data points with lower limits on  $N_{\text{CIV}}/N_{\text{OVI}}$  much greater than unity, which is no surprise. Our high-metallicity clouds typically have  $N_{\text{CIV}} \lesssim 10^{13}$  which means that such points would need to have  $N_{\text{OVI}} \ll 10^{13}$  which is much lower than the typical contamination in the O VI region. We would also not expect this region to

be populated by C IV absorbers because it corresponds to densities beyond the peak in the C IV fraction.

If the absorbers are photo-ionized, then we can obtain a lower limit on the density by shifting the points either upwards (which would imply O VI is contaminated but N V is not) or to the right (implying N V is contaminated but O VI is not), until they fall on top of the rightmost solid curve which corresponds to  $\log T = 4.0$ . For the metal-rich clouds the median, required shift in the column density ratio is a modest 0.42 dex. However, if both  $N_{\text{OVI}}$  and  $N_{\text{NV}}$  are contaminated, then the required shifts will be greater. In fact, even in the absence of contamination this should be the case because the presence of noise implies that our  $1\sigma$  upper limits on the N V and O VI column densities typically exceed the true values. The resulting lower limit on the density (upper limit on the ionization parameter) is very robust, because taking a temperature high enough for collisional ionization to become important yields higher densities (to compensate for the enhanced ionization).

### 5.1 Method

We use the following procedure to constrain the physical parameters of the absorbers.

First, we make several assumptions: (1) the absorbers are exposed to the  $z = 2.3$  Haardt & Madau (2001) model for the meta-galactic radiation field; (2) the relative abundances of the heavy elements are solar; (3) the gas is in ionization equilibrium; (4) the gas temperature is  $\log[T(\text{K})] = 4.0$ . In §5.3 we will discuss both the validity of these assumptions and the effects of relaxing them.

Second, we use our measurements of  $N_{\text{CIV}}$  and our upper limits on  $N_{\text{NV}}$  and  $N_{\text{OVI}}$  to obtain lower limits on two column density ratios (C IV/N V and C IV/O VI), which provide us with two lower limits on the density. The greater of these two lower limits is then our best estimate of the lower limit on the gas density. Figure 5 shows how the inferred density varies as a function of these and other column density ratios.

Third, we obtain an upper limit on the size of the absorbers. The absorber radius is given by

$$R = \frac{1}{2} \frac{N_{\text{HI}}}{n_{\text{HI}}}. \quad (5)$$

Since the neutral hydrogen fraction increases monotonically with density, our lower limit on the density gives us also a lower limit on  $n_{\text{HI}}$ , the density of neutral hydrogen. Together with our measured upper limit on  $N_{\text{HI}}$ , we thus obtain an upper limit on  $R$ . Figure 5 (right  $y$ -axis) shows how the inferred radius varies as a function of the column density ratios.

Fourth, we obtain an upper limit on the abundance of silicon relative to carbon. Analogously to equation (2), we can write this relative abundance as

$$\begin{aligned} [\text{Si}/\text{C}] &= \log\left(\frac{N_{\text{SiIV}}}{N_{\text{CIV}}}\right) - \log\left(\frac{n_{\text{SiIV}}/n_{\text{Si}}}{n_{\text{CIV}}/n_{\text{C}}}\right) - \log\left(\frac{n_{\text{Si}}}{n_{\text{C}}}\right)_{\odot} \\ &= \log\left(\frac{N_{\text{SiIV}}}{N_{\text{CIV}}}\right) - \log\left(\frac{N_{\text{SiIV}}}{N_{\text{CIV}}}\right)_{\odot, n_{\text{H}}}, \end{aligned} \quad (6)$$

where the last term denotes the predicted column density ratio  $N_{\text{SiIV}}/N_{\text{CIV}}$  for solar abundances and the density,  $n_{\text{H}}$ , appropriate for the particular absorber. In other words, if we

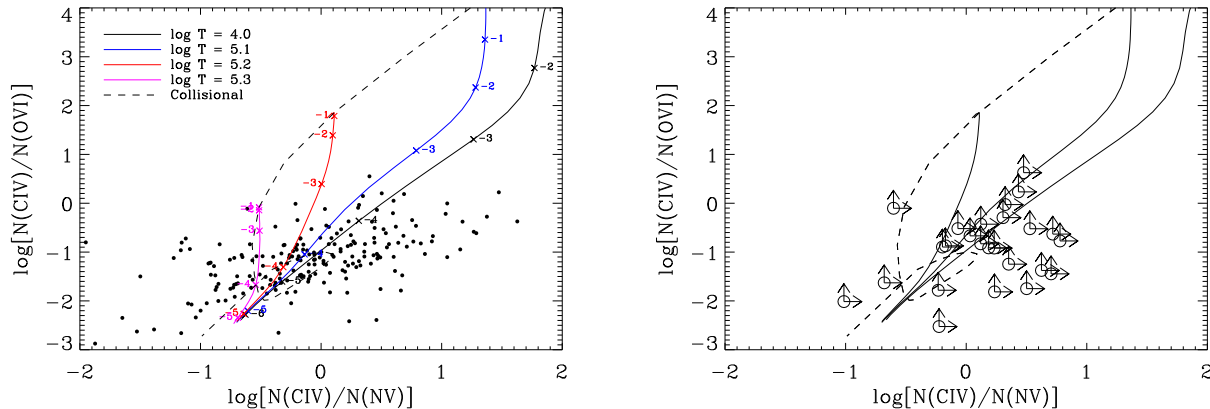


**Figure 4.** Measured  $1\sigma$  lower limit on the column density ratio  $N(\text{CIV})/N(\text{OVI})$  versus the  $1\sigma$  lower limit on the ratio  $N(\text{CIV})/N(\text{NV})$  for all CIV absorbers (*left*) and for the metal-rich components only (*right*). The curves indicate the predicted ratios assuming solar abundances and the  $z = 2.3$  Haardt & Madau (2001) model of the UV/X-ray background from quasars and galaxies. Density varies along the solid curves (values of  $\log[n_{\text{H}}(\text{cm}^{-3})]$  are indicated), but the temperature is kept fixed at (*right-to-left*)  $\log[T(\text{K})] = 4.0, 5.1, 5.2,$  and  $5.3,$  respectively. Temperature varies along the dashed curve, which assumes pure collisional ionization equilibrium (and is therefore independent of the density). Parts of curves for which  $n(\text{CIV})/n(\text{C}) < 10^{-6}$  are not plotted. Three data points are missing from the plot on the right: one to the left and two below the plotted range, many more are missing from the panel on the left (compare with Fig. 2). In the left panel the arrows have been suppressed for clarity.

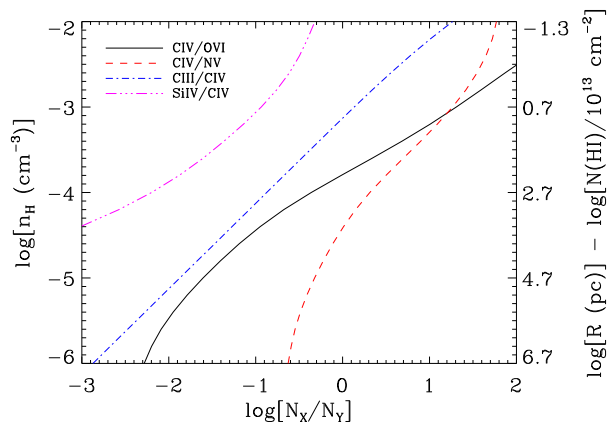


**Figure 5.** Hydrogen number density as a function of column density ratio for CIV/OVI (*solid*), CIV/NV (*dashed*), CIII/CIV (*dot-dashed*), and SiIV/CIV (*dot-dot-dot-dashed*), respectively. The  $y$ -axis on the right-hand side indicates the corresponding cloud radius for  $N_{\text{HI}} = 10^{13} \text{ cm}^{-2}$  (the inferred radius is proportional to the measured HI column density).

know the gas density, then  $[\text{Si}/\text{C}]$  is just the difference between the measured value of  $\log(N_{\text{SiIV}}/N_{\text{CIV}})$  and the value predicted for solar abundances. Since we have measured an upper limit on  $N_{\text{SiIV}}$ , we can obtain an upper limit on  $[\text{Si}/\text{C}]$  provided we have a lower limit on  $(N_{\text{SiIV}}/N_{\text{CIV}})_{\odot, n_{\text{H}}}$  [or, equivalently, an upper limit on  $(n_{\text{CIV}}/n_{\text{C}})/(n_{\text{SiIV}}/n_{\text{Si}})$ ]. As the dot-dot-dot-dashed curve in figure 5 shows, our lower limit on the density gives us precisely this.

Finally, for those absorbers for which CIII falls in the wavelength range covered by our spectra, we perform a consistency check using our upper limit on  $N_{\text{CIII}}$ . Since CIII/CIV is a monotonically increasing function of the density (see Fig. 5, *dot-dashed* curve), our upper limit on

$N_{\text{CIII}}/N_{\text{CIV}}$  translates into an upper limit on the density which does not rely on any assumption about relative abundances. For each absorber we check whether the upper limit derived from CIII is greater than the lower limit derived from NV and OVI. Naturally, the actual values for the upper limits are also of great interest.

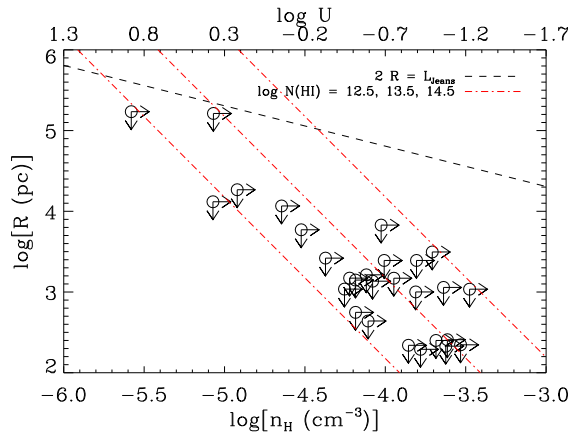
## 5.2 Results

Table 4 gives the results of the ionization models for all 28 high-metallicity clouds.

Figure 6 shows the upper limits on the size as a function of the lower limits on the density (upper limits on the ionization parameter, upper  $x$ -axis). The median upper limit on the radius is  $\log[R(\text{pc})] = 3.2$  and the median lower limit on the gas density is  $\log[n_{\text{H}}(\text{cm}^{-3})] = -4.0$ . Had we only made use of CIV/NV (CIV/OVI), then the median lower limit on the density would have been  $-4.2$  ( $-4.4$ ). For comparison, the results for the complete sample of CIV absorbers are  $\log R < 5.3$  and  $\log n_{\text{H}} > -4.4$ . Thus, while the upper limits on the density are similar for ordinary and metal-rich CIV absorbers, our upper limits to the sizes are two orders of magnitude smaller for the high-metallicity clouds.

There appears to be an anti-correlation between the upper limits on the size and the lower limits on the density. The dot-dashed lines, which indicate contours of  $\log[N_{\text{HI}}(\text{cm}^{-2})] = 12.5, 13.5,$  and  $14.5,$  respectively, show that this anti-correlation is directly related to the relatively small range in neutral hydrogen columns covered by our data.

The absence of points in the bottom-left half of the diagram could be due to a selection effect: such points correspond to neutral hydrogen columns less than  $10^{12.5} \text{ cm}^{-2}$  or a central optical depth of less than 0.07 (for a  $b$ -value of  $35 \text{ km s}^{-1}$  which is the line width corresponding to  $b_{\text{CIV}} = 10 \text{ km s}^{-1}$  for thermal broadening). The severe blending of



**Figure 6.** Inferred  $1\sigma$  upper limits on the radius as a function of the inferred  $1\sigma$  lower limits on the gas density (bottom  $x$ -axis) and ionization parameter (top  $x$ -axis) for all absorbers listed in Table 3. The median upper limit on the radius is  $\log[R(\text{pc})] < 3.2$  and the median lower limit on the gas density is  $\log[n_{\text{H}}(\text{cm}^{-3})] = -4.0$ . Note that the points cannot be shifted onto the dashed line, which indicates the radius-density relation for self-gravitating gas clouds, because the inferred radius decreases faster with increasing density than the Jeans scale (see text for details).

$\text{Ly}\alpha$  lines and the presence of noise in the data generally do not allow us to put such tight constraints on the HI column densities. The absence of points in the upper-right part of the diagram is a bit more difficult to explain. This region corresponds to  $\log N_{\text{HI}} > 14.5$ . To pass our selection criterion, such points would need to have very high CIV column densities, which are rare. However, one selection effect that may play a role here, is that such HI lines are strongly saturated which often results in weak constraints on  $N_{\text{HI}}$  and hence on the metallicity.

As we already discussed, the upper limits on  $N_{\text{NV}}$  and  $N_{\text{OVI}}$ , from which the lower limit on the density is derived, are likely dominated by contamination. Hence, the scatter in the density may not be real. Since  $R \propto n_{\text{HI}}^{-1} \propto n_{\text{H}}^{-2}$  (assuming a highly ionized plasma in photoionization equilibrium), systematic errors in  $n_{\text{H}}$  would give rise to a spurious  $R \propto n_{\text{H}}^{-2}$  anti-correlation parallel to the contours of constant  $N_{\text{HI}}$ , which is close to the observed scaling.

The dashed curve in Figure 6 shows the Jeans scale (for a purely gaseous cloud), which is the expected size for a self-gravitating cloud and which is also similar to the size of typical  $\text{Ly}\alpha$  forest absorbers (Schaye 2001),

$$L_J \sim 6.5 \times 10^4 \text{ pc} \left( \frac{n_{\text{H}}}{10^{-4} \text{ cm}^{-3}} \right)^{-1/2} \left( \frac{T}{10^4 \text{ K}} \right)^{1/2} f_g^{1/2}, \quad (7)$$

where  $f_g$  is the fraction of the mass in gas. All of our metal-rich clouds are constrained to be smaller than the Jeans scale and many by a large factor. Note that this conclusion cannot be avoided by shifting the data points to the right, because an increase in the density would result in an even larger decrease in the size:  $R \propto n_{\text{HI}}^{-1}$  which scales with  $n_{\text{H}}^{-2}$  if the gas is highly ionized and with  $n_{\text{H}}^{-1}$  if it is neutral. This dependence is steeper than that for the Jeans length, which scales as  $L_J \propto n_{\text{H}}^{-1/2}$ . Thus, increasing the density makes the clouds less gravitationally bound.

If the clouds were self-gravitating, then their masses would need to be strongly dominated by stars and/or dark matter. Setting  $2R = L_J$  and solving for the gas fraction, we obtain a median upper limit on the gas fraction of  $\log f_g < -3.2$ . If we do the same for the complete sample of CIV absorbers, we obtain  $\log f_g < 0.7$  which is consistent with self-gravity for ordinary gas fractions. Hence, the metal-rich clouds appear to differ from the general population in that they are either not gravitationally confined, or have negligible gas fractions.

For 15 of our high-metallicity clouds our spectra cover the CIII region, enabling us to measure an upper limit on CIII/CIV and thus on the density. Reassuringly, for all clouds the upper limits are consistent with the lower limits shown in figure 6, which were determined independently from the CIV/NV and CIV/OVI ratios. If we repeat the analysis for the full sample of 179 CIV components for which we can measure upper limits on  $N_{\text{CIII}}$ , we again find that every upper limit is greater than the corresponding lower limit on the density (the minimum difference is in that case 0.02 dex). This gives us confidence in the robustness of the constraints obtained from the ionization models.

The median upper limit is  $\log n_{\text{H}} = -3.0$ , exactly one order of magnitude above the median lower limit. The minimum difference between the upper and lower limits is 0.5 dex. This result suggests that  $\log n_{\text{H}} \approx -3.5$  is a reasonable estimate for the typical gas density. Because  $R \propto n_{\text{H}}^{-2}$ , this would mean that the upper limit on the size should typically be reduced by an order of magnitude, which would give a median value of  $\log R < 2.2$ . Note that this is still an upper limit, insofar as it is based on an upper limit on  $N_{\text{HI}}$ . Finally, the median upper limit on the gas fraction would be reduced to  $\log f_g < -4.5$ .

Assuming the clouds are roughly spherical, we can estimate their gas masses. Typical values are

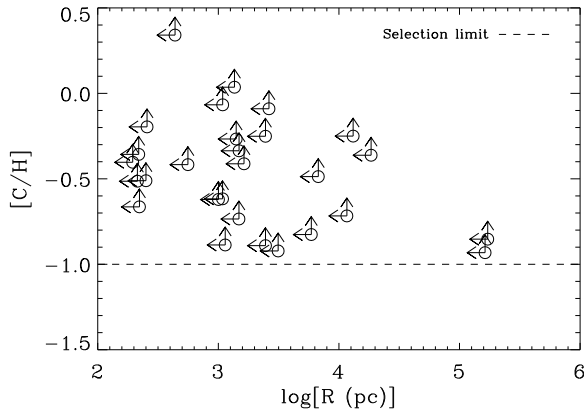
$$\begin{aligned} M_g &\sim \frac{4\pi}{3} \frac{n_{\text{H}} m_{\text{H}} R^3}{X}, \\ &\sim 4 \times 10^1 M_{\odot} \left( \frac{n_{\text{H}}}{10^{-3.5} \text{ cm}^{-3}} \right) \left( \frac{R}{10^2 \text{ pc}} \right)^3, \end{aligned} \quad (8)$$

where we assumed a hydrogen mass fraction  $X = 0.75$ . We emphasize that the mass is much more poorly constrained than the size, because  $M_g \propto R^3$ .

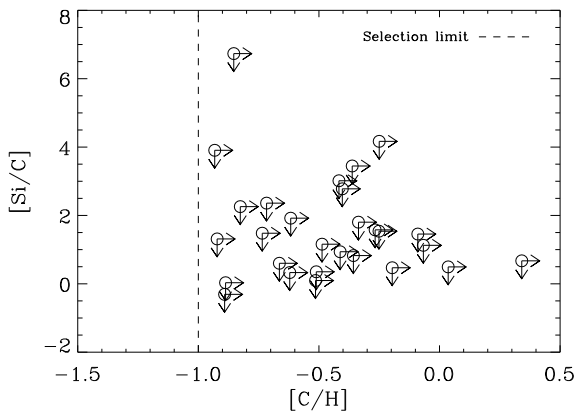
In Figure 7 we plot the metallicity as a function of the cloud size. By selection, the clouds have relatively high metallicities: the median lower limit is  $Z > 0.4Z_{\odot}$ , which is much greater than the metallicities typical of the low-density IGM. The absence of large, metal-rich clouds has the same origin, whatever it is, as the absence of points in the upper, right part of figure 6. Because the inferred limits on the metallicity and size scale as  $Z \propto N_{\text{HI}}^{-1} \propto R^{-1}$  [see equations (2) and (5)], an anti-correlation between  $Z$  and  $R$  is not unexpected.

Figure 8 shows that for all but one cloud the abundance of silicon relative to that of carbon and oxygen is consistent with the solar value level. The median upper limit is not particularly interesting:  $[\text{Si}/\text{C}] < 1.5$  which reflects the fact that we do not expect to detect SiIV in these clouds (they are too small and too low-density).

We conclude that our metal-rich ( $Z \gtrsim Z_{\odot}$ ) clouds are typically moderately overdense,  $n_{\text{H}} \sim 10^{-3.5} \text{ cm}^{-3}$ , which is



**Figure 7.** Inferred  $1\sigma$  lower limits on the metallicity as a function of the inferred  $1\sigma$  upper limits on the radius for all absorbers listed in Table 3. The median lower limit on the metallicity is  $[C/H] > -0.42$  and the median upper limit on the radius is  $\log[R(\text{pc})] < 3.2$ .



**Figure 8.** Inferred  $1\sigma$  upper limits on the abundance of silicon relative to carbon as a function of the inferred  $1\sigma$  lower limits on the metallicity for all systems listed in Table 3. The median upper limit on the relative abundance of silicon is  $[Si/C] < 1.5$  and the median lower limit on the metallicity is  $[C/H] > -0.42$ .

about 50 times greater than the mean density at  $z = 2.25$ , and compact,  $R \sim 10^2$  pc. They are too small relative to their densities for them to be gravitationally confined, unless their stars and/or dark matter outweigh the gas by more than four orders of magnitude.

### 5.3 Uncertainties

In this section we will investigate how robust our conclusions are with respect to the assumptions on which our ionization models rely. We will show that our qualitative conclusions, namely that the clouds are compact, not self-gravitating, and have high metallicities, are robust. In particular, we will show that these conclusions would be strengthened if: the radiation field were harder and/or more intense, oxygen were overabundant relative to carbon, the heavy elements were not yet in ionization equilibrium (which we will ar-

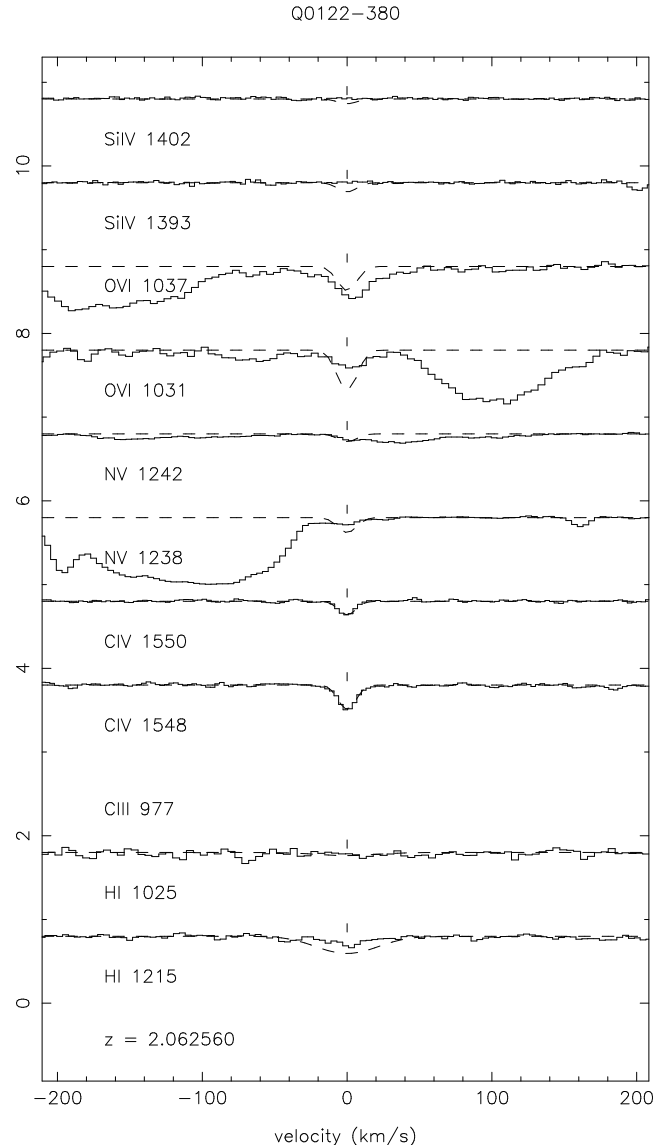


**Figure 9.** The system at  $z = 2.062560$  in Q0122 – 380 showing (from bottom-to-top) the HI Ly $\alpha$ , HI Ly $\beta$ , CIII, CIV, NV, OVI, and SiIV regions on a velocity scale centered on the redshift given at the bottom of the figure. The profiles corresponding to the upper limits on the column densities are shown as dashed lines. An integer offset has been applied to separate the different transitions. Both lines of the CIV doublet are clearly present, and there are blended features which may contain the NV and OVI lines. Ly $\alpha$  is weak, but present.

gue may be true), and if the temperature were high enough for collisional ionization to be important (we will, however, argue that this is unlikely to be the case).

The main caveat appears to be the possibility of a much softer radiation field, which would result in larger clouds and, for a subset of the absorbers, lower metallicities. However, in practice a significantly softer radiation field would require the presence of local, soft sources (galaxies) and the resulting increase in the hydrogen ionization rate would decrease the inferred cloud sizes. Moreover, we shall argue that the rates of incidence of the metal-rich absorbers is too high for local sources to dominate the radiation field.

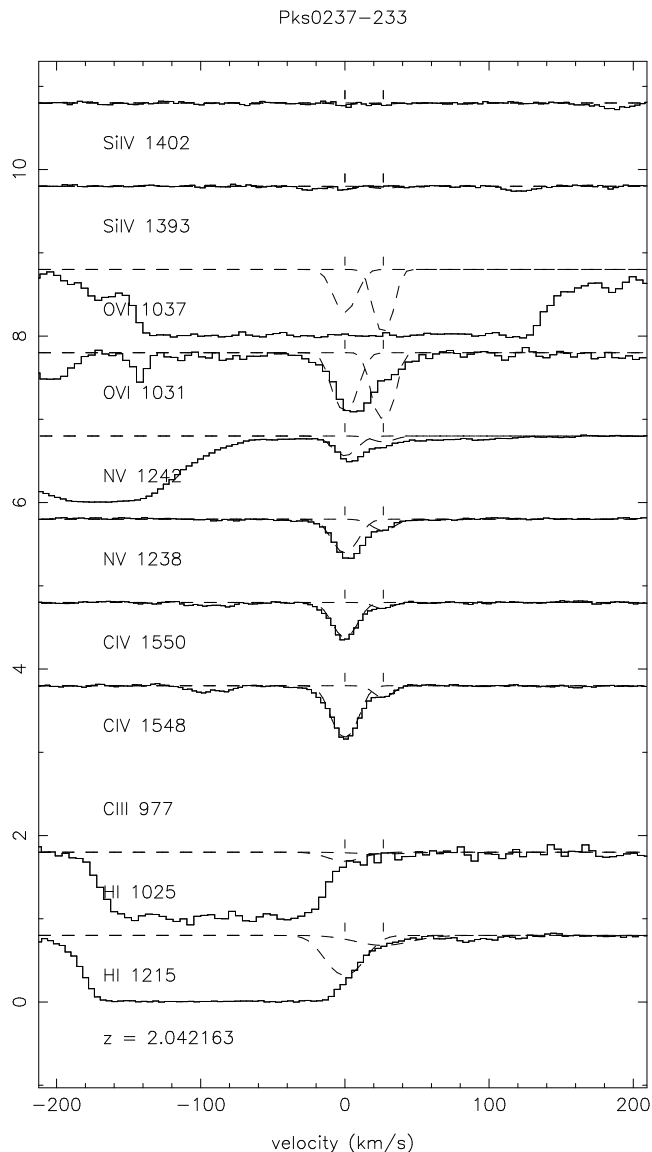


**Figure 10.** The  $z = 2.042163$  and  $2.042433$  components in Pks0237–333. C IV and NV are clearly present, the weaker O VI component is strongly contaminated. Ly $\alpha$  falls in the wing of a strong HI system.

### 5.3.1 The radiation field

We assumed that the clouds are exposed to the integrated UV/X-ray radiation from quasars and galaxies, as computed by Haardt & Madau (2001) for  $z = 2.3$ . Given that the metal-rich clouds are unlikely to be gravitationally confined and that they have high metallicities, it would perhaps not be surprising if they resided in the environments of galaxies. In that case the local radiation could be both more intense and softer than the background (which includes a substantial contribution from quasars).

Schaye (2006, see also Miralda-Escudé 2005), showed that under the assumption that the absorbers reside in the halos of the sources that dominate the ionizing background, the ratio of the mean flux from local sources to the flux from the background is given by

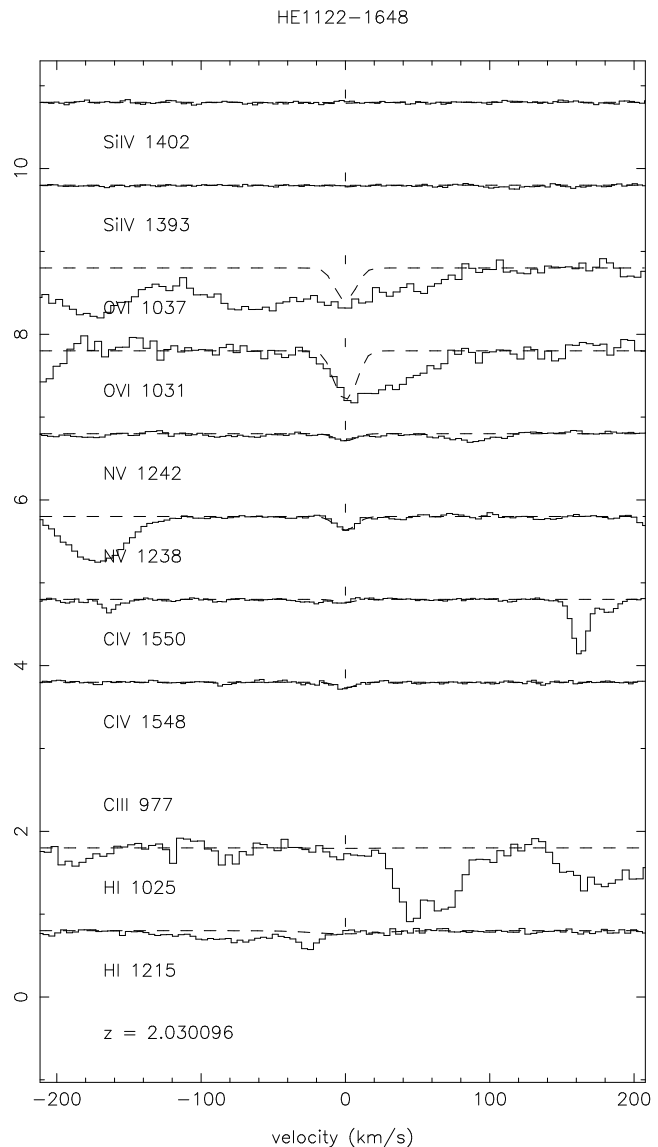


**Figure 11.** The system at  $z = 2.030096$  in HE1122–1648. This system was described and analyzed by Carswell et al. (2002). C IV and NV are clearly present, O VI is strongly contaminated, and HI is very weak.

$$\frac{\bar{F}}{F_{\text{bg}}} = \left(\frac{dN}{dz}\right)_{\text{crit}} \left(\frac{dN}{dz}\right)^{-1}, \quad (9)$$

where the critical rate of incidence is given by

$$\left(\frac{dN}{dz}\right)_{\text{crit}} \approx 0.6 \frac{\langle f_{\text{esc},N} \rangle f_{\text{cov}}}{f_{\text{esc}}}, \quad (10)$$

where  $f_{\text{esc},N}$  and  $f_{\text{esc}}$  are the fractions of the locally emitted radiation that is able to escape to the absorber and out of the halo of the galaxy, respectively,  $f_{\text{cov}}$  is the covering factor, and we assumed that the rate of incidence of Lyman limit systems per unit redshift is 1.3 (Péroux et al. 2005) and that the HI column density distribution has the form  $dN/dz \propto N_{\text{HI}}^{-1.5}$ . Since the HI columns of our absorbers are much smaller than those typical of galaxies, we expect  $f_{\text{esc},N} \approx f_{\text{esc}}$ . The covering factor is unlikely to be much smaller than unity given that more than half of our systems contain multiple high-metallicity clouds. Plugging

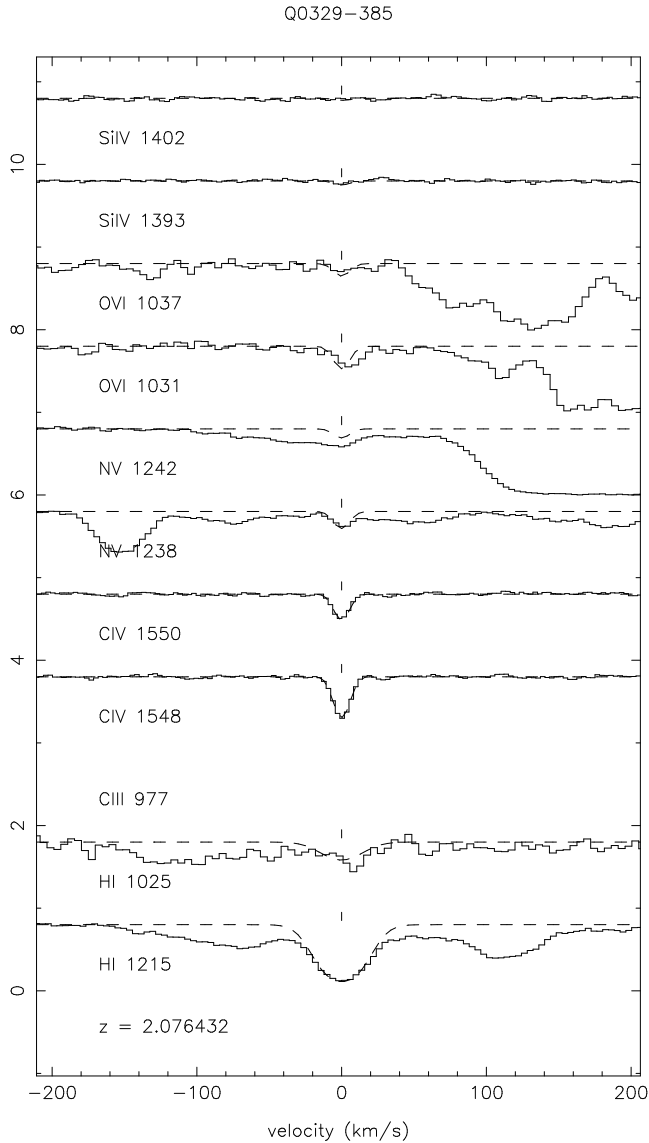


**Figure 12.** The  $z = 2.076432$  system in Q0329 – 385. CIV has corresponding unsaturated Ly $\alpha$  and probably weak NV. The O VI doublet is noisy, but not strongly contaminated.

in our system rate of incidence ( $dN/dz = 3$ ), which is really a lower limit given our conservative approach, we find that  $\bar{F}/F_{\text{bg}} \lesssim 0.2$ . Thus, in general we do not expect local sources to dominate the ionizing radiation field to which our absorbers are exposed.

We will nevertheless examine the consequences of changes in the intensity and spectral hardness, because we cannot be sure that the Haardt & Madau (2001) model is an accurate description of the ionizing background. As discussed in §5, from observed column density ratios such as CIV/O VI, we can, under certain assumptions, measure the ionization parameter. Assuming that we know the intensity  $I$  of the ionizing radiation field, we can translate this into a gas density. From equations (4) and (5) it can be seen that if the intensity  $I$  of the radiation were higher, the clouds would be denser and smaller:  $n_{\text{H}} \propto I$  and  $R \propto I^{-1}$  (for a fixed ionization parameter the neutral hydrogen fraction is independent of the intensity, therefore  $R \propto n_{\text{H}}^{-1} \propto n_{\text{H}}^{-1} \propto I^{-1}$ ).

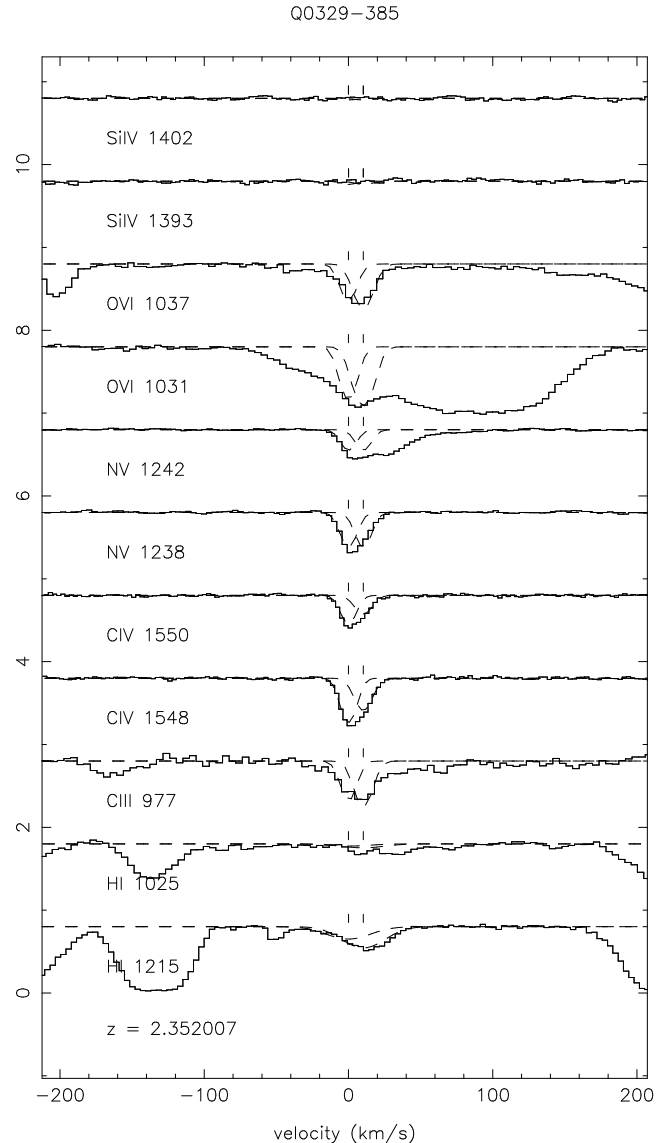


**Figure 13.** The  $z = 2.352007$  and  $2.352122$  components in Q0329 – 385. The systems show clear CIV and NV. O VI 1031 is contaminated. Ly $\alpha$  is also clearly distinguishable, but with the apparent dominant component offset in velocity from the heavy element lines.

Both the metallicity and the relative abundance of silicon would remain unchanged, as can be seen from figure 1 and equation (6) (column density ratios depend on the ionization parameter rather than the density).

Changing the spectral hardness of the radiation will affect the inferred properties in the following way. Since the ionization potentials of O V and N IV are higher than that of C III (114 and 77 versus 48 eV), softer spectra yield higher CIV/O VI and CIV/N V ratios. Thus, if the true radiation field is softer than the Haardt & Madau (2001) model, we will have overestimated the lower limit on the density, underestimated the size, and overestimated the relative abundance of silicon (see Fig. 5). A softer radiation field would, however, decrease the C III/C IV ratio, which would give us higher upper limits on the density. For 26 of the 28 clouds the constraint on the metallicity would remain unchanged,

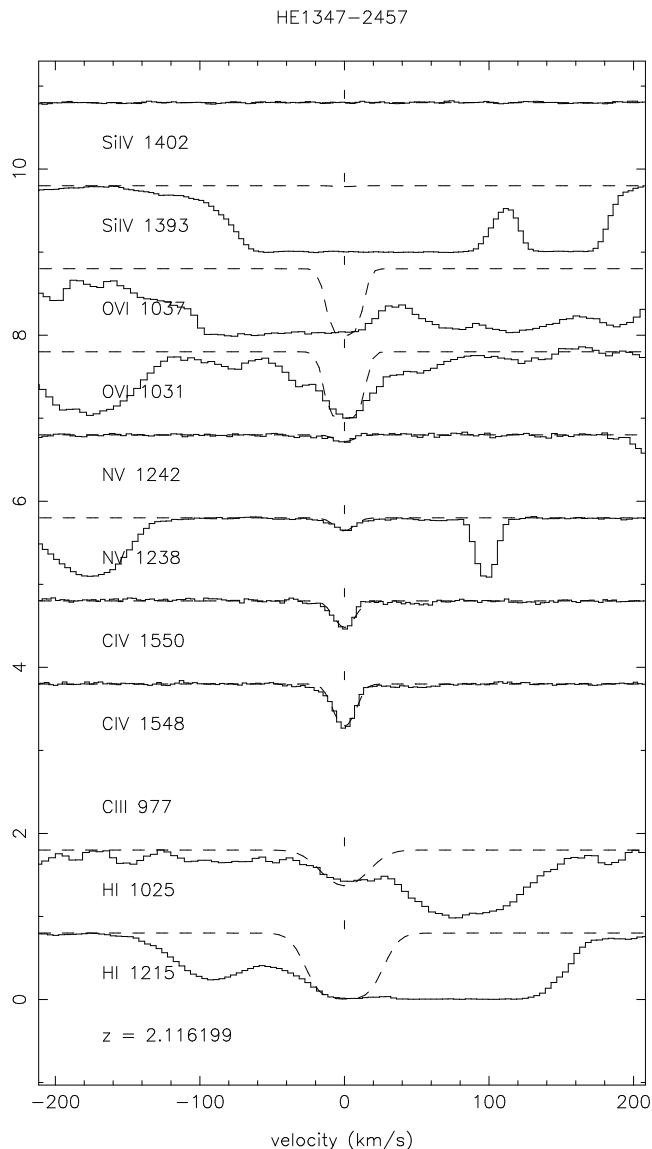


**Figure 14.** The system at  $z = 2.116199$  in HE1347–2457. CIV and NV are present, but OVI is strongly contaminated. At  $\log N_{\text{HI}} < 14.1$ , this is one of the strongest Ly $\alpha$  lines in our sample. There is a stronger Ly $\alpha$  line at  $+81 \text{ km s}^{-1}$  for which no associated heavy elements are detected.

because for these we assumed  $n_{\text{CIV}}/n_{\text{HI}}$  to have its maximum possible value. The remaining 2 clouds could drop out of our sample because the curves in figure 2 would shift to the right. Conversely, if the radiation field were harder, we would infer higher densities, smaller sizes, lower silicon abundances and, in some cases, higher metallicities (which could also lead to an increased sample size). Note that a much harder radiation field would lead to inconsistencies between the lower limits on the density inferred from CIV/OVI and CIV/NV and the upper limits derived from CIII/CIV.

If, contrary to the prediction of Schaye (2006), radiation from local galaxies were important for our absorbers, then the radiation would have a softer spectral shape, but it would also be more intense than in our fiducial model. This means that the effects on the density and the size would be difficult to predict.

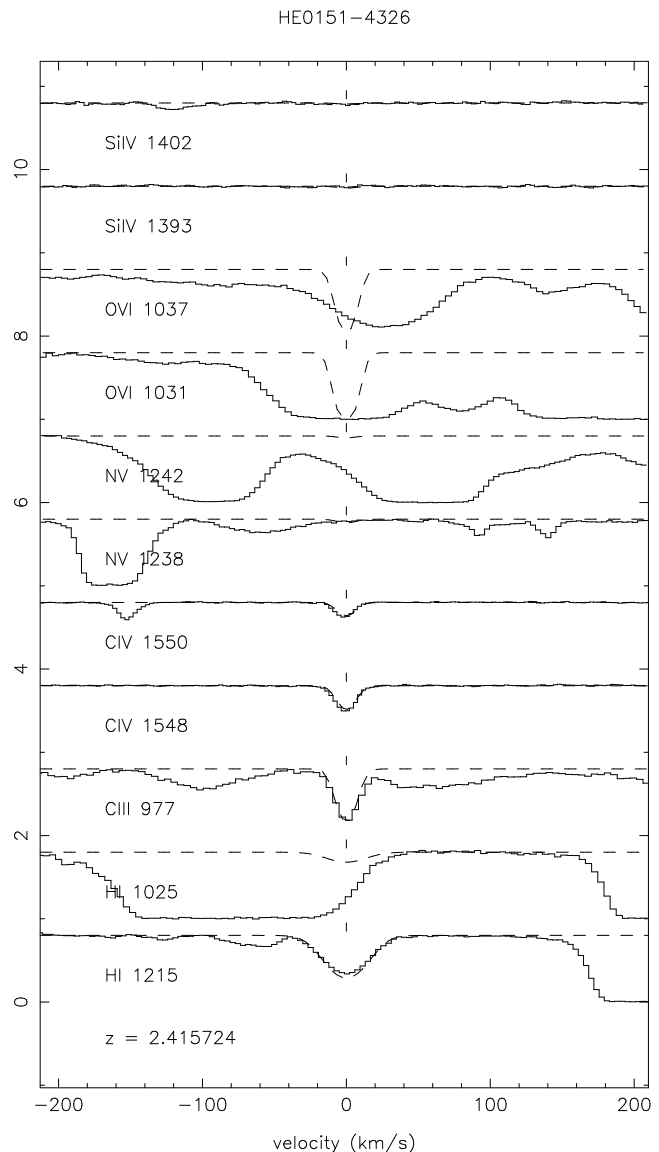


**Figure 15.** The  $z = 2.415724$  component of the system at  $z = 2.417$  in HE0151–4326. The other component of this system is shown in Fig. 16. HI, CIII and both CIV lines are clearly seen, there is a tight upper limit on NV, but OVI is strongly contaminated.

### 5.3.2 Relative abundances

We assumed that the relative abundances of carbon, nitrogen, and oxygen are the same as for the sun. However, at high redshift oxygen is often found to be overabundant relative to carbon (e.g., Telfer et al. 2002), while nitrogen is often underabundant, at least relative to oxygen (e.g., Bergeron et al. 2002). On the other hand, since nitrogen and carbon are both produced by intermediate stars, we may expect  $[\text{N}/\text{C}]$  to be close to solar. Furthermore, it is likely that the relative abundances of the elements are a stronger function of metallicity than of time, in which case we would expect the relative abundances to be close to solar, because the metallicity of the clouds is typically of order solar.

Nevertheless, let us examine the consequences of extreme variations in the assumed relative abundances. We

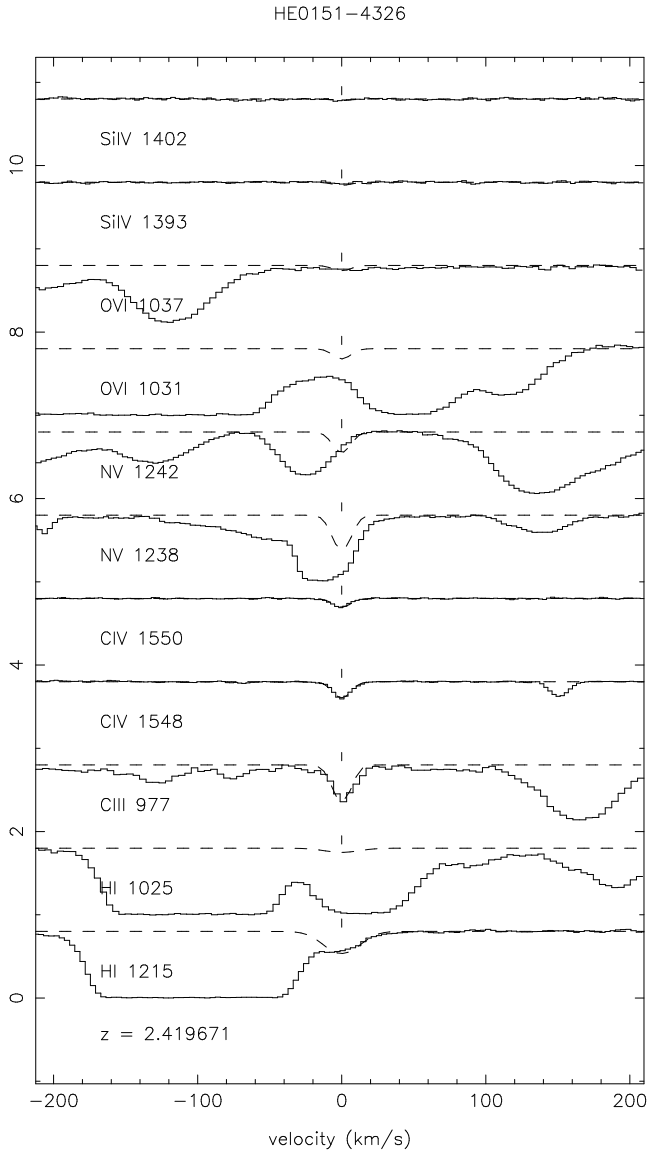


**Figure 16.** The  $z = 2.419671$  component of the system at  $z = 2.417$  in HE0151–4326. The other component of this system is shown in Fig. 15. HI falls in the wing of a strong system. C III and both C IV lines are clearly seen. NV is strongly contaminated, but there is a tight upper limit on O VI.

find that increasing the abundance of oxygen relative to that of carbon by a factor of 10, leads to the addition of three clouds to our sample (but no new systems), while decreasing the N/C ratio by a factor of 10 removes one cloud (and one system) from the sample. Increasing O/C (decreasing N/C) by an order of magnitude increases (decreases) the median lower limit on the density by 0.4 (0.3) dex, leaves the upper limits on the density nearly unchanged, decreases (increases) the median upper limit on the size by 0.8 (0.4) dex, increases (decreases) the median lower limit on the metallicity by 0.5 (0.4) dex, and decreases (increases) the median upper limit on the relative abundance of silicon by 0.7 (0.7) dex. Thus, increasing O/C has the opposite effect of decreasing N/C, but the results tend to be more sensitive to O/C.

We conclude that even extreme changes in the assumed relative abundances would not change our conclusions. In

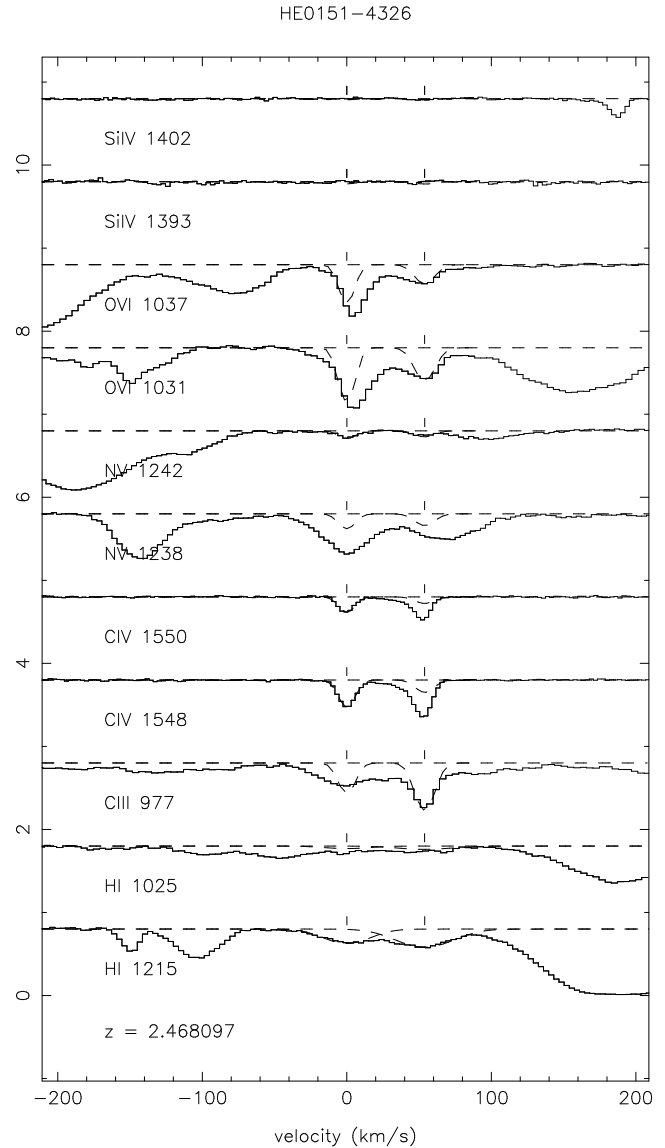


**Figure 17.** The  $z = 2.468097$  and  $2.468720$  components in Q0151–4326. For CIV and O VI it is clear that these components are blended with others, which however, did not pass the selection criteria. Both NV and O VI appear to allow measurements of upper limits that are relatively free from contamination by HI. The O VI lines are significantly broader than the corresponding CIV lines.

fact, the most natural modification (enhanced oxygen relative to carbon), would make the metal-rich clouds even more dense, compact, and metal-rich.

### 5.3.3 Ionization equilibrium

We assumed the gas to be in ionization equilibrium. However, if the clouds were created by gas cooling from high temperatures, this assumption could temporarily break down because for  $T \sim 10^5 - 10^6$  K the cooling time can be much shorter than the relevant photoionization (and recombination) timescales of the metals (some of these timescales exceed  $10^8$  yr). Thus, if the clouds were created hot,  $T \gg 10^4$  K, and have lifetimes  $t \lesssim 10^8$  yr, then they may be much

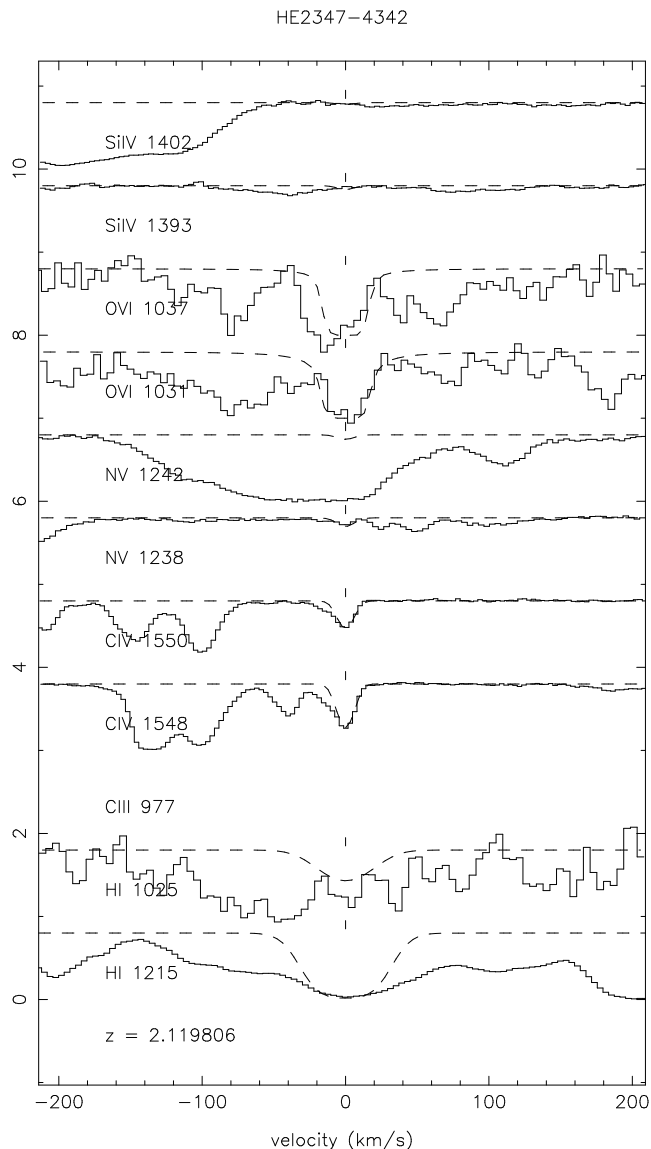


**Figure 18.** The  $z = 2.119806$  system at in HE2347–4342. Most of the absorption just to the left of the CIV system is in fact NV at  $z = 2.8968 - 2.8984$ , in the quasar proximity zone. The effective continuum in the HI Ly $\beta$  and O VI regions was reduced to account for Lyman limit absorption.

more highly ionized than they would be in photoionization equilibrium. The ionization balance of the metals would then be similar to that of collisionally ionized gas, even though the clouds would typically have temperatures of  $T \sim 10^4$  K. However, since for hydrogen the photoionization timescale is only  $\sim 10^4$  yr, ionization equilibrium is likely to be a very good approximation for this element. Below we will investigate how the properties of the clouds would change if the heavy elements had not yet reached photoionization equilibrium.

As discussed in §5, the column density ratios CIV/O VI and CIV/NV decrease with the degree to which the gas is ionized, which means they increase with density in photoionization equilibrium. By assuming photoionization equilibrium, we may thus have underestimated the gas density. The cloud size was computed using  $R = N_{\text{HI}}/2n_{\text{HI}}$  which,

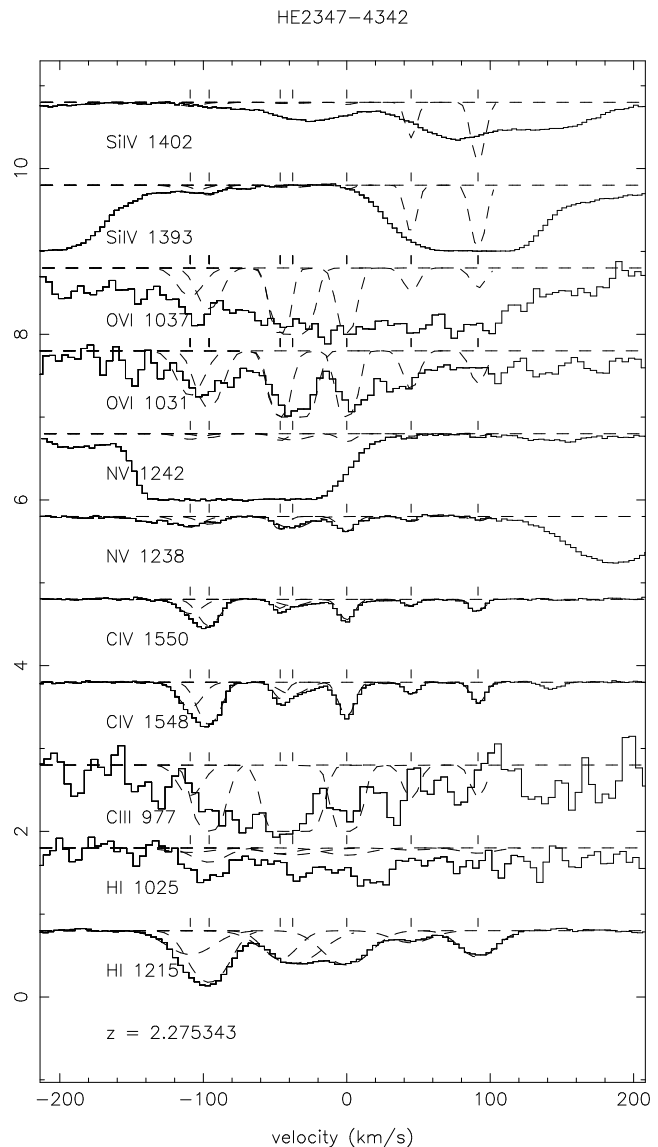


**Figure 19.** The  $z = 2.274151, 2.274295, 2.274836, 2.274931, 2.275343, 2.275833,$  and  $2.276343$  components from the system at  $z = 2.275$  in HE2347–4342. The effective continuum in the HI Ly $\beta$ , C III, and O VI regions was reduced to account for Lyman limit absorption. Complex absorption by HI, CIV, and NV is clearly visible.

making use of the fact that hydrogen is likely to be close to photoionization equilibrium (i.e.,  $n_{\text{HI}}/n_{\text{H}} \propto n_{\text{H}}$ ), implies  $R \propto n_{\text{H}}^{-2}$ . Hence, we may have overestimated the cloud size.

The effects on the abundances are somewhat more difficult to predict. From equation (2) we can see that  $10^{[\text{C}/\text{H}]} \propto (n_{\text{HI}}/n_{\text{H}})(n_{\text{CIV}}/n_{\text{C}})^{-1} \propto n_{\text{H}}(n_{\text{CIV}}/n_{\text{C}})^{-1}$ , where number densities are computed assuming solar abundances and we assumed that hydrogen is in photoionization equilibrium (i.e.,  $n_{\text{HI}} \propto n_{\text{H}}^2$ ). Given that CIV/O VI and CIV/NV are good “ionization meters”, our estimate of the ratio CIV/C is probably roughly right despite the fact that we assumed ionization equilibrium. However, the equilibrium assumption will have caused us to underestimate the gas density and thus the metallicity.

If we assume that the equilibrium model that best

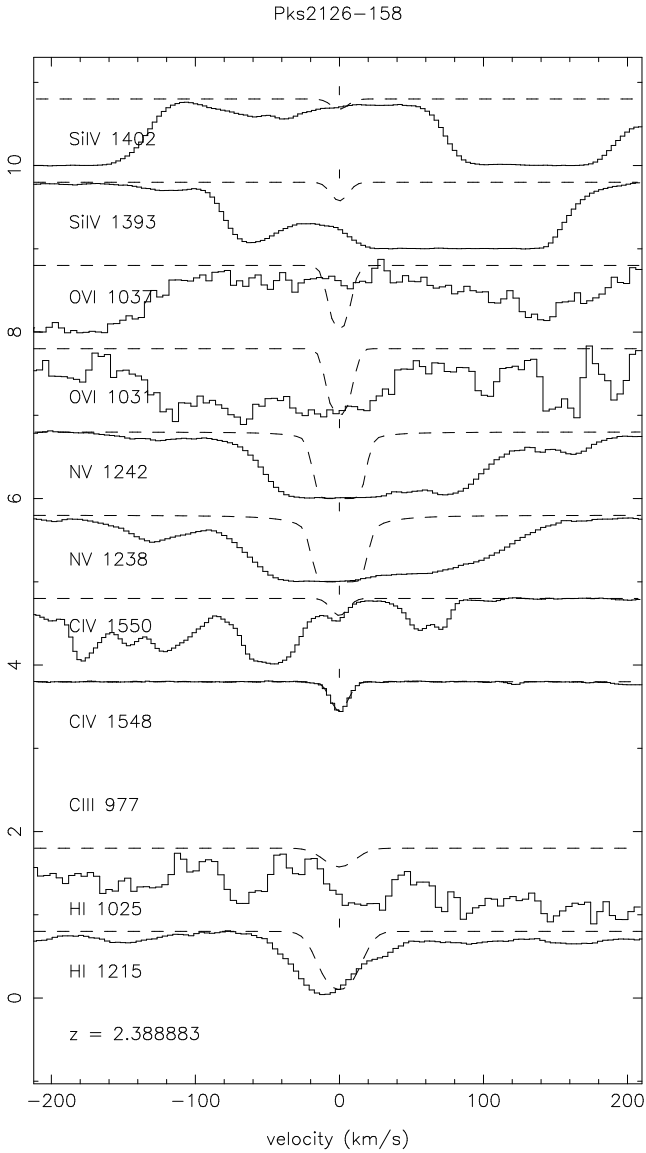


**Figure 20.** The  $z = 2.388883$  component of the  $z = 2.394$  system in Pks2126–158. The other components of this system are shown in Fig. 21. HI Ly $\beta$ , NV, O VI, and Si IV all suffer from strong contamination.

fits the measured column density ratios CIV/O VI and CIV/N V predicts approximately the right Si IV/CIV ratio, then it follows from equation (6) that the inferred relative abundance of silicon is unaffected by the assumption of ionization equilibrium.

In short, if the clouds were created hot and are short-lived, then the heavy elements might not yet be in photoionization equilibrium. In that case our conclusions would again be strengthened: we would have underestimated the limits on the density, substantially overestimated the upper limit on the size, probably underestimated the lower limit on the metallicity, and probably inferred roughly the right upper limit on [Si/C].

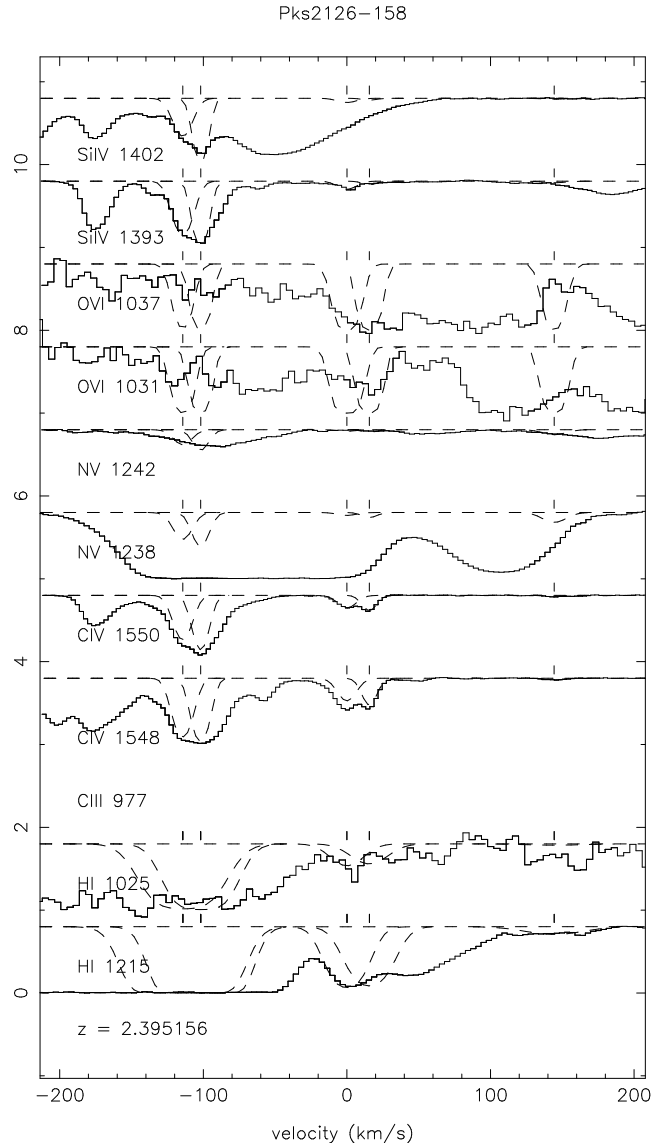


**Figure 21.** The  $z = 2.393862$ ,  $2.394003$ ,  $2.395156$ ,  $2.395333$ , and  $2.396791$  components of the  $z = 2.394$  system in Pks2126–158. The other component of this system is shown in Fig. 20. HI Ly $\beta$  and O VI are very noisy. NV 1242 provides tight upper limits.

### 5.3.4 Temperature

We chose to keep the temperature fixed rather than assume thermal equilibrium because the cooling rate depends on the metallicity and on the dynamical state of the clouds, which we do not know a priori. We assumed that the clouds have a temperature  $T = 10^4$  K, which is typical of a photo-ionized plasma and means that collisional ionization is unimportant.

Figure 4 demonstrates that the metal column density ratios are insensitive to the temperature as long as  $T \sim 10^4$  K. For  $T \gtrsim 10^5$  K, collisional ionization becomes increasingly important and the gas gets more highly ionized. The dashed curves in figure 4 indicate the predicted column density ratios for the artificial case of pure collisional ionization equilibrium (temperature is varied along these curves).

From Figure 4 it can clearly be seen that the data do not favor temperatures high enough for collisional ionization

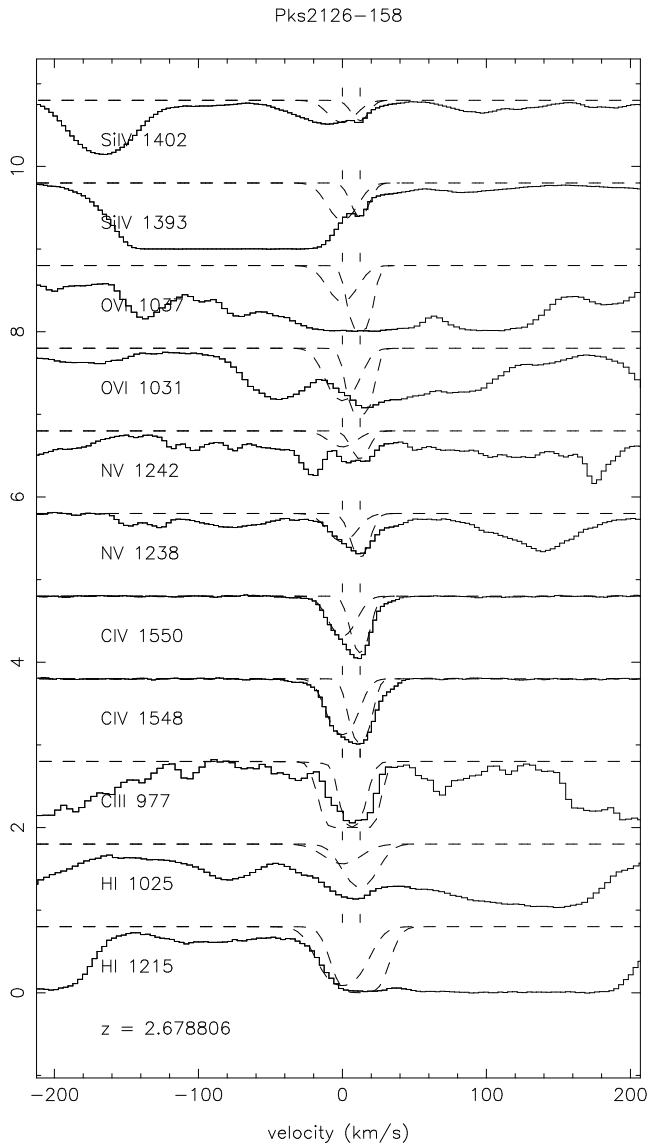


**Figure 22.** The  $z = 2.678806$  and  $2.678957$  components of the  $z = 2.679$  system in Pks2126–158. Strong HI and very strong CIV are clearly present. NV is probably also present. OVI is strongly contaminated.

to be important. Bringing the high-temperature models into agreement with the data requires much larger shifts of the data points. In fact, most limits are incompatible with the  $\log T = 5.2$  and  $5.3$  models. For the (unrealistic) case of pure collisional ionization, which corresponds to the high density limit in the presence of an ionizing background, all but 4 points can be shifted onto the dashed curve, but this would imply that for most absorbers the upper limit on  $N_{\text{OVI}}$  exceeds the true value by more than 2 orders of magnitude and that most have nearly identical temperatures. Thus, it appears the data favor photo-ionization over collisional processes.

This conclusion is further strengthened by the measured CIV line widths. For collisional ionization to be effective, temperatures of  $T \gtrsim 10^5$  K are required, corresponding to line widths of

$$b = 40.5 \text{ km s}^{-1} \left( \frac{m_{\text{H}}}{m} \right)^{1/2} \left( \frac{T}{10^5 \text{ K}} \right)^{1/2}. \quad (11)$$

As can be seen from Table 3 (col. 11), more than half of the CIV lines are sufficiently narrow to rule out such high temperatures.

In short, several independent pieces of evidence suggest that most of the metal-rich clouds are at temperatures too low for collisional ionization to be important.

Nevertheless, let us examine the effect of a higher temperature. If the gas were hot enough for collisional ionization to be important, then the gas would be more highly ionized. As discussed in §5.3.3, this would imply that we have underestimated the limits on the densities. As discussed in §3, the metallicities would generally remain unaffected, although the lower limits would be slightly reduced if  $\log T$  were within about 0.2 dex of 5.05. For  $\log T = (4.85, 5.05, 5.25)$  we find (10,6,10) metal-rich systems and (24, 7, 18) metal-rich clouds. The median lower limit on the density is increased by (0.2,0.2,0.5) dex, the median upper limit on the size is increased by (0.3,0.4,0.3) dex, and the median lower limit on the metallicity is decreased by (0.2, 0.4, 0.2) dex. If we increase the temperature further, then we find many more high-metallicity systems and clouds, and we require much denser and compact clouds.

To summarize, if the gas has a temperature high enough for the metals to be collisionally ionized ( $T \gtrsim 10^5$  K), which we argued is unlikely, then our conclusions are generally strengthened: we find more metal-rich clouds and infer higher densities and smaller sizes. Only for temperatures very close to  $\log T = 5.05$  do we find somewhat fewer metal-rich clouds and infer slightly weaker constraints on the sizes (but stronger constraints on the densities).

## 6 DISCUSSION

In the previous sections we showed that at  $z \approx 2.3$  there exists a population of highly ionized, metal-rich gas clouds that give rise to CIV absorption in the spectra of quasars. These clouds often come in groups, but some appear isolated. Some are located close to strong HI absorbers, but others are not. Groups of high-metallicity clouds have a rate of incidence  $dN/dz > 3.0 \pm 0.9$ , while the rate for individual clouds is  $dN/dz > 7 \pm 1$ . Their densities are typically  $n_{\text{H}} \sim 10^{-3.5} \text{ cm}^{-3}$ , they have sizes  $R \sim 10^2$  pc, and metallicities  $Z \gtrsim Z_{\odot}$ .

What could the high-metallicity clouds be? Intergalactic supernovae remnants, interplanetary planetary nebulae, (fragments of) shells driven by galactic superwinds, dark matter minihalos, high-velocity clouds, tidally stripped gas? We note that many of the possible origins have been discussed in related contexts, such as weak Mg II systems (e.g., Rigby et al. 2002; Milutinovic et al. 2006 and references therein) and strong OVI absorbers (e.g., Simcoe et al. 2006; Bergeron & Herbert-Fort 2005), and that some of the arguments used in those studies can also be applied to the high-metallicity CIV clouds. In the rest of this section we will discuss some of these scenarios in passing, but we will focus on questions that can be addressed without knowledge of the origin of the clouds.

### 6.1 Cosmological significance

It is interesting to investigate the cosmological significance of the high-metallicity clouds. In this section we derive some generic results that are independent of the interpretation of the nature of the population. Our starting point will be the observed rates of incidence and the typical physical properties derived from the ionization model. In each case we will show how the results scale with these and other parameters.

Let  $n$  be the *comoving* number density of clouds and let each cloud provide a *proper* cross section  $\pi R^2$ . The total rate of incidence is then given by

$$\frac{dN}{dz} = n\pi R^2 \frac{c}{H(z)} (1+z)^2. \quad (12)$$

Using  $(\Omega_m, \Omega_\Lambda, h) = (0.3, 0.7, 0.7)$  and  $z = 2.3$  we find,

$$n \approx 1.6 \times 10^4 \text{ Mpc}^{-3} \left( \frac{dN/dz}{7} \right) \left( \frac{R}{10^2 \text{ pc}} \right)^{-2}. \quad (13)$$

Comparing this with the number of bright Lyman-Break Galaxies (LBG) at  $z = 3$ ,  $n_g \sim 10^{-2} h^3 \text{ Mpc}^{-3}$  down to  $0.1L_*$  (Steidel et al. 1999), it is clear that the population of clouds must be enormous: the high-metallicity clouds outnumber bright galaxies by about a million to one.

Conversely, if we assume that the clouds reside in the environments of a population of objects with comoving number density  $n_g$ , we can estimate the proper radius,  $r_h$ , of the halo containing high-metallicity clouds around each such object,

$$r_h \approx 8.3 \times 10^4 \text{ pc} \left( \frac{dN/dz}{3} \right)^{1/2} \left( \frac{n_g}{10^{-2} \text{ Mpc}^{-3}} \right)^{-1/2} f_{\text{cov}}^{-1/2}, \quad (14)$$

where  $f_{\text{cov}}$  is the covering factor of high-metallicity clouds in the halo and  $dN/dz = 3$  is the rate of incidence of metal-rich systems (as opposed to clouds). Given that there are typically multiple high-metallicity clouds per system, we expect  $f_{\text{cov}}$  to be of order unity. If the clouds are related to galactic winds, we would expect galaxies fainter than  $0.1L_*$  to contribute too, since winds may escape more easily from small galaxies. Therefore, the halos containing metal-rich clouds could typically be smaller than  $10^2$  kpc. Interestingly, simulations predict that at  $z \sim 3$ , superwinds driven by starbursting galaxies manage to propagate to scales  $\lesssim 10^2$  kpc (Aguirre et al. 2001).

The product of the comoving number density and the cloud mass gives us the cosmic gas mass density of the high-metallicity clouds. Expressed in units of the critical density this becomes

$$\begin{aligned} \Omega &= \frac{nM_g}{\rho_{\text{crit}}}, \\ &\approx 5.2 \times 10^{-6} \left( \frac{dN/dz}{7} \right) \left( \frac{R}{10^2 \text{ pc}} \right) \left( \frac{n_{\text{H}}}{10^{-3.5} \text{ cm}^{-3}} \right). \end{aligned} \quad (15)$$

Note that if the absorption were to arise in shells centered on galaxies rather than in spherical clouds, the total mass contained in the population would be about the same (the mass of a shell exceeds that of a spherical cloud by a factor of about  $(r/R)^2$ , where  $r$  is the radius of the shell, but the number density of shells is down by the same factor relative to that of spherical clouds). Comparing the cosmic gas density of the high-metallicity clouds to the cosmic baryon density  $\Omega_b \approx 0.044$  (e.g., Spergel et al. 2003), we see that the

population of metal-rich clouds contains a negligible fraction of the baryons.

The high-metallicity clouds account for a cosmic metallicity of

$$Z_{\text{cosmic}} = \frac{\Omega Z}{\Omega_b}, \quad (16)$$

$$\begin{aligned} &\approx 1.2 \times 10^{-4} Z \left( \frac{dN/dz}{7} \right) \left( \frac{R}{10^2 \text{ pc}} \right) \\ &\quad \times \left( \frac{n_{\text{H}}}{10^{-3.5} \text{ cm}^{-3}} \right), \end{aligned} \quad (17)$$

where  $Z$  is the cloud metallicity. Comparing this estimate to the total carbon abundance in the diffuse ( $\delta < 10^2$ ) IGM inferred from CIV absorbers,  $[C/H] = -2.8$  (S03, for their fiducial UV background model), we find that the clouds contain of order 10% of the intergalactic metals associated with detectable CIV absorption.

In §6.4.1 we will show that the cosmological significance of the clouds would be drastically increased if the clouds are short-lived, as we will argue is likely to be the case.

### 6.2 Cloud confinement

There are in general two ways to confine a gas cloud: gravity and external pressure. We already showed that gravitational confinement of the high-metallicity clouds is only possible if the gas mass is negligible. Below we will explore this possibility, as well as confinement by external pressure. We will show that gravitational confinement by dark matter minihalos with mass  $M \sim 10^6 - 10^7 M_\odot$  would be possible, except that there probably are not enough minihalos to account for the large number of high-metallicity clouds. We will also show that confinement by external pressure is generally only possible if the confining medium has an overdensity of a few or less and a temperature greater than  $10^5$  K.

#### 6.2.1 Self-gravity

In §5.2 we found that for the high-metallicity clouds to be self-gravitating, the median gas mass fraction would have to be smaller than  $\log f_g < -3.2$ . This estimate was based on the lower limits on the densities derived from the lower limits on the column density ratios CIV/N V and CIV/O VI, and the upper limits on the cloud sizes obtained by combining the upper limits on  $N_{\text{HI}}$  and the lower limits on the densities. However, the observed upper limits on  $N_{\text{CIII}}/N_{\text{CIV}}$  suggested that the densities are typically about 0.5 dex greater than our lower limits, which in turn reduces the upper limits on the sizes by 1 dex. From equation (7) we can see that the gas fraction required for gravitational confinement then becomes

$$f_g \sim 7.7 \times 10^{-6} \left( \frac{n_{\text{H}}}{10^{-3.5} \text{ cm}^{-3}} \right) \left( \frac{R}{10^2 \text{ pc}} \right)^2 T_4^{-1}, \quad (18)$$

where  $T_4 \equiv T/(10^4 \text{ K})$ . Using equation (9) this gives a total mass of

$$M \sim 5.7 \times 10^6 M_\odot \left( \frac{R}{10^2 \text{ pc}} \right) T_4. \quad (19)$$

Note that the required total mass is much less uncertain than the gas mass, which scales as  $M_g \propto n_{\text{H}} R^3$ .

If we identify the total mass with the virial mass of a halo collapsing at redshift  $z_c$ , then we find a virial radius of

$$r_{\text{vir}} \sim 1.2 \times 10^2 \text{ pc} \left( \frac{R}{10^2 \text{ pc}} \right)^{1/3} T_4^{1/3} \left( \frac{1+z_c}{11} \right)^{-1}, \quad (20)$$

which agrees remarkably well with the characteristic size we inferred from the ionization modeling ( $R \sim 10^2 \text{ pc}$ ) if the halo collapsed at high redshift. Such a halo would have a circular velocity of

$$v_c \equiv \left( \frac{GM}{r_{\text{vir}}} \right)^{1/2} \quad (21)$$

$$\sim 15 \text{ km s}^{-1} \left( \frac{R}{10^2 \text{ pc}} \right)^{1/3} T_4^{-1/6} \left( \frac{1+z_c}{11} \right)^{1/2},$$

and a virial temperature of

$$T_{\text{vir}} \equiv \frac{\mu m_{\text{H}} v_c^2}{3k} \quad (22)$$

$$\sim 5.0 \times 10^3 \text{ K} \left( \frac{R}{10^2 \text{ pc}} \right)^{2/3} T_4^{-1/3} \left( \frac{1+z_c}{11} \right).$$

Since the virial temperature is smaller than  $10^4 \text{ K}$ , stars could only have formed in such a minihalo if it collapsed before reionization.

The comoving number density of minihalos is  $n(M > 10^6 M_{\odot}) \sim 10^{2.6} \text{ Mpc}^{-3}$  at  $z = 10$ , increasing to about  $10^3$  at  $z = 6$  (e.g., Reed et al. 2007). This is significantly lower than the comoving number density of high-metallicity clouds, which we estimated to be  $2 \times 10^4 \text{ Mpc}^{-3}$  [see eq. (13)]. The discrepancy is actually worse, since many of the minihalos that collapsed before reionization will have merged with galaxies by  $z = 2.3$  and it is only the remainder that we should consider here. We therefore do not think that minihalos from reionization can account for a significant fraction of the high-metallicity clouds.

### 6.2.2 External pressure

We have two useful constraints on a possible confining medium: it must have about the same pressure as the clouds and it must give rise to HI absorption that is consistent with our upper limit on the HI column density.

The high-metallicity clouds have only a modest pressure,

$$\frac{P}{k} = nT \sim 10^{0.5} \text{ cm}^{-3} \text{ K} \left( \frac{n_{\text{H}}}{10^{-3.5} \text{ cm}^{-3}} \right) T_4. \quad (23)$$

This pressure is relatively well constrained because much higher densities are ruled out by our upper limits on the C III/C IV ratio and much higher temperatures are inconsistent with the line widths as well as the metal column ratios (see §5.3.4). If the confining medium has a higher density, then this would imply a temperature smaller than  $10^4 \text{ K}$ . Such low temperatures are only expected for clouds that are optically thick to ionizing radiation, which is clearly ruled out by our constraints on  $N_{\text{HI}}$ .

A higher temperature, on the other hand, would imply an overdensity lower than 50, which means that the medium would have a density significantly lower than is typical of virialized objects. This is, however, certainly not impossible. The confining gas could for example have been heated

by accretion shocks onto large-scale filaments or by shocks associated with galactic winds. The medium must, however, be sufficiently hot that collisional ionization suppresses its neutral hydrogen absorption to the very low levels we observe.

Figure 23 shows as solid contours the typical neutral hydrogen column density (*left*) and HI Ly $\alpha$  optical depth at the line center (*right*) associated with a self-gravitating ( $2R = L_J$ ) gas cloud as a function of its gas density and temperature. The dashed lines are lines of constant pressure, corresponding to  $P/k = 10^0$  and  $10^1 \text{ cm}^{-3} \text{ K}$ , respectively. The region enclosed by the dashed lines roughly satisfies the pressure constraint. To be consistent with the observed HI absorption we typically require<sup>7</sup>  $N_{\text{HI}} \ll 10^{13} \text{ cm}^{-2}$  or, for  $T \gg 10^5 \text{ K}$ ,  $\tau_c \ll 10^{-1}$  (note that the column density constraint was inferred under the assumption that  $b_{\text{HI}} = (m_{\text{C}}/m_{\text{H}})^{1/2} b_{\text{CIV}}$ ). A confining medium with  $n_{\text{H}} \sim 10^{-5} \text{ cm}^{-3}$  and  $T \sim 10^{5.5} \text{ K}$  would satisfy all constraints. In general, the density cannot be high compared with the cosmic mean and the temperature must exceed  $10^5 \text{ K}$ .

If the confining medium is not self-gravitating, as could for example be the case if it were expanding, hot, wind fluid, then its size will be smaller than in the hydrostatic equilibrium case, making it possible to satisfy the absorption constraints for higher densities.

### 6.3 Lifetimes

If the clouds are confined neither by self-gravity nor by external pressure, as seems plausible from the above discussion, then they will freely expand until they reach pressure equilibrium with their environment.

The free expansion timescale is just the ratio of the cloud size and internal sound speed  $c_s$ ,

$$t_{\text{exp}} \sim \frac{R}{c_s} = R \sqrt{\frac{\mu m_{\text{H}}}{\gamma k T}} \quad (24)$$

$$\sim 6.4 \times 10^6 \text{ yr} \left( \frac{R}{10^2 \text{ pc}} \right) T_4^{-1/2},$$

where we used a mean particle weight  $\mu = 0.59$  and a ratio of specific heats  $\gamma = 5/3$ . The expansion timescale is very small compared to the Hubble time, which means that the high-metallicity clouds may be a transient phenomenon.

In fact, the clouds would likely be short-lived, even in the presence of a confining medium. Unless it is gravitationally confined, a cloud of size  $R$  and density  $\rho$  that is moving with velocity  $v$  relative to a medium with density  $\rho_{\text{m}}$ , will be destroyed through Kelvin-Helmholtz and Rayleigh-Taylor instabilities on a timescale (e.g., Jones, Kang, & Tregillis 1994)

$$t_{\text{inst}} \sim \left( \frac{\rho}{\rho_{\text{m}}} \right)^{1/2} \frac{R}{v}, \quad (25)$$

which we can write as

<sup>7</sup> We are assuming that the HI absorption is dominated by the high-metallicity cloud. If it were dominated by a confining medium, then the high-metallicity clouds would have metallicities  $Z \gg Z_{\odot}$  and sizes  $R \ll 10^2 \text{ pc}$ .

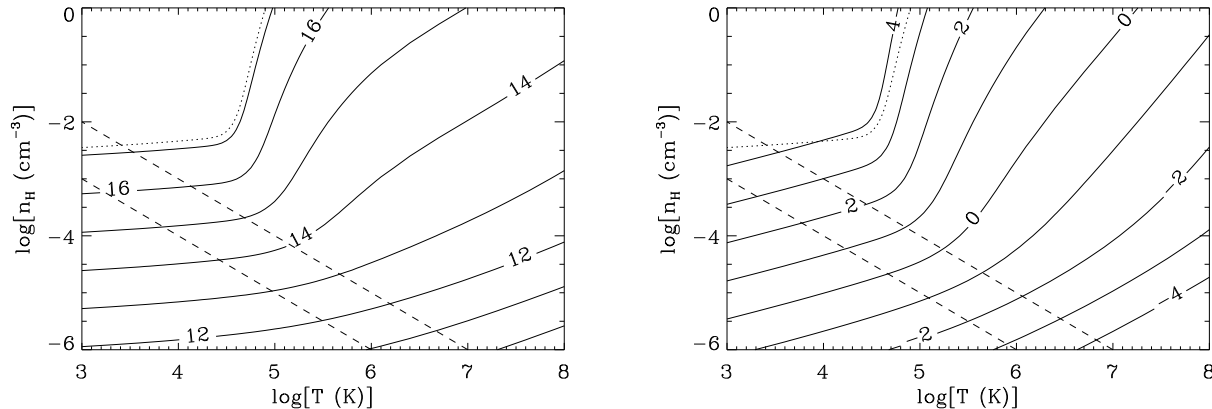


**Figure 23.** Typical HI column densities and Ly $\alpha$  optical depths expected for self-gravitating clouds as a function of the cloud density and temperature. The solid curves are contours of constant neutral hydrogen column density (*left*) and HI Ly $\alpha$  optical depth at the line center (*right*). The dotted contours indicate the self-shielding limit,  $\log[N_{\text{HI}} (\text{cm}^{-2})] = 17.2$ , and the dashed contours correspond to pressures of  $\log[P/k (\text{cm}^{-3}\text{K})] = 0$  (*bottom*) and 1 (*top*). The cloud was exposed to the Haardt & Madau model for the  $z = 2.3$  UV/X-ray background and assumed to be optically thin.

$$t_{\text{inst}} \sim t_{\text{exp}} \left( \frac{\rho}{\rho_m} \right)^{1/2} \frac{c_s}{v} \sim t_{\text{exp}} \left( \frac{P}{P_m} \right)^{1/2} \frac{c_{s,m}}{v}, \quad (26)$$

where  $c_s$  is the internal sound speed of the cloud and  $c_{s,m}$  is the sound speed in the confining medium. If the cloud is falling into or rotating within a hot, hydrostatic gaseous halo, then we would expect  $v \sim c_{s,m}$  in which case the cloud will be destroyed in an expansion timescale if the medium has a pressure similar to that of the cloud. In general,  $t_{\text{inst}} \gg t_{\text{exp}}$  would require  $v \ll c_{s,m}$  for pressure-confined clouds. Since the cloud has an overdensity of only about 50 and the medium is unlikely to be underdense by a large factor, we expect  $c_{s,m} \lesssim \sqrt{50}c_s$ . Thus,  $v \ll c_{s,m}$  would imply velocities of only a few km/s, which seems implausible. Note that the clouds would have to be born with such small velocities because, as we will show below, deceleration from  $v \sim c_s$  takes longer than  $t_{\text{inst}}$ . Clouds could perhaps form with such small relative velocity if they formed from an expanding, hot wind fluid. However, in that case the cloud lifetime would still be limited by the free expansion timescale of the wind fluid, which is typically much smaller than the Hubble time. We conclude that hydrodynamical instabilities would likely change the cloud on a timescale similar to the expansion timescale.

Note that although two-dimensional magnetohydrodynamic simulations have shown that magnetic fields inhibit the disruption of supersonic clouds through fluid instabilities (Mac Low et al. 1994), three-dimensional simulations show that the interaction with a magnetic field perpendicular to the direction of motion actually accelerates the development of the Rayleigh-Taylor instability (Gregori et al. 1999).

Unless the cloud is driven by ram-pressure, for example in the form of a galactic wind, a moving cloud will decelerate on the timescale that it sweeps up its own mass,

$$t_{\text{dec}} \sim \frac{\rho}{\rho_m} \frac{R}{v} \sim t_{\text{exp}} \frac{\rho}{\rho_m} \frac{c_s}{v}. \quad (27)$$

For clouds that are denser than their environment this exceeds  $t_{\text{inst}}$ , which means that deceleration due to conserva-

tion of momentum cannot save the cloud from being disrupted.

Note that free expansion will not lead to temperatures much lower than  $10^4$  K because the photo-heating timescale becomes extremely short at such low temperatures for highly ionized clouds<sup>8</sup>. For example, for  $T = 10^3$  K and  $n_{\text{H}} \sim 10^{-3.5} \text{ cm}^{-3}$  the photo-heating timescale is more than an order of magnitude smaller than the timescale for adiabatic cooling resulting from free expansion<sup>9</sup>.

In summary, we expect the clouds to be short-lived, with a characteristic lifetime of order the free expansion timescale, equation (25).

## 6.4 Implications of short lifetimes

If the high-metallicity clouds are short-lived, as we argued is likely, then this has important implications for their cosmological significance as well as for scenarios accounting for their origin.

### 6.4.1 Cosmological significance

If the high-metallicity clouds are short-lived, then the amount of metal contained in the population at any given time is much smaller than the total amount of metal that has passed through such a phase. Assuming a steady population of freely expanding clouds, the total cosmic metallicity that has gone through the phase corresponding to the high-metallicity clouds is of order

$$Z_{\text{cosmic}} \frac{t_H}{t} \approx 5.2 \times 10^{-2} Z \left( \frac{t}{10^7 \text{ yr}} \right)^{-1} \left( \frac{dN/dz}{7} \right) \quad (28)$$

<sup>8</sup> If the clouds went through an optically thick phase, then they may have been colder in the past.

<sup>9</sup> Radiative cooling is extremely inefficient below  $10^4$  K for a photo-ionized plasma.

$$\times \left( \frac{R}{10^2 \text{ pc}} \right) \left( \frac{n_{\text{H}}}{10^{-3.5} \text{ cm}^{-3}} \right).$$

If the lifetime  $t \propto R$ , as in equation (25), then this estimate is independent of the cloud size and lifetime.

Comparing this again to the metallicity of the diffuse IGM,  $Z/Z_{\odot} \sim 10^{-2.8} \sim 1.6 \times 10^{-3}$  if carbon is used as a tracer (S03), we see that if the clouds are short-lived, all of the carbon contained in the IGM could in principle at one time have resided in high-metallicity clouds. Note, however, that many of the high metallicity clouds may end up inside galaxies and that the same gas could be cycled through multiple generations of high-metallicity clouds.

#### 6.4.2 The nature of the clouds

Galactic winds are a plausible origin for the high-metallicity clouds. Both observations and simulations show that the wind fluid is highly clumpy (e.g., Veilleux et al. 2005). Hot gas sweeps up shells which fragment due to thermal and hydrodynamical instabilities. The hot gas pushes itself out in between the fragments, sweeping up new shells in the process. Shell fragments are constantly being formed and destroyed.<sup>10</sup> Hence, the lifetimes of individual clouds may be much shorter than the duration of the wind phenomenon (which could, in fact, exceed the Hubble time). It is easy to see that this would indeed be necessary for the high-metallicity clouds.

Starbursting galaxies at high redshift are observed to generate outflows with velocities of  $v \sim 10^2 - 10^3 \text{ km s}^{-1}$  (e.g., Pettini et al. 1998). Hence, we would expect the typical age of a metal-rich halo of size  $r_h$  to be at least

$$t = 9.8 \times 10^7 \text{ yr} \left( \frac{r_h}{10^4 \text{ pc}} \right) \left( \frac{v}{10^2 \text{ km s}^{-1}} \right)^{-1} \quad (29)$$

$$\sim 8.1 \times 10^8 \text{ yr} \left( \frac{dN/dz}{3} \right)^{1/2} f_{\text{cov}}^{-1/2} \quad (30)$$

$$\times \left( \frac{n_g}{10^{-2} \text{ Mpc}^{-3}} \right)^{-1/2} \left( \frac{v}{10^2 \text{ km s}^{-1}} \right)^{-1},$$

where we used equation (14) in the last step. Unless the galaxy number density  $n_g \gg 10^{-2} \text{ Mpc}^{-3}$  or the (sustained) wind velocity  $v \gg 10^2 \text{ km s}^{-1}$ , the travel time exceeds the characteristic cloud lifetime  $t_{\text{exp}} \sim 10^7 \text{ yr}$  [equation (25)]. In the wind scenario this would suggest that the clouds are continuously being destroyed and formed. Comparing the wind propagation timescale with the minimum age of a starburst,  $\sim 10^7 \text{ yr}$  (i.e., the lifetime of a  $8 M_{\odot}$  star), we see that if high-metallicity clouds arise in the winds of starbursting galaxies, the associated galaxies may already have faded by the time their winds have expanded into the regime of our high-metallicity clouds.

The high-metallicity clouds could also be part of individual, intergalactic supernova remnants. For example, Shel-

ton (1998) showed using non-equilibrium models of supernova remnants expanding in the lower Galactic halo that such objects can give rise to high ionization lines such as the ones associated with our high-metallicity CIV clouds.

If each component is associated with a single, distinct supernova remnant, then the population traces a comoving star formation rate density of:

$$\dot{\rho}_* = 10^2 n M_{100} / t \quad (31)$$

$$\sim 1.6 \times 10^{-1} M_{\odot} \text{ Mpc}^{-3} \text{ yr}^{-1} M_{100} \left( \frac{dN/dz}{7} \right) \quad (32)$$

$$\times \left( \frac{r}{10^2 \text{ pc}} \right)^{-2} \left( \frac{t}{10^7 \text{ yr}} \right)^{-1},$$

where  $r$  and  $t$  are the radius and age of the remnant, respectively, and  $M_{100}$  is the average mass in stars for which the initial mass function predicts a single supernova. We used as default values the ones appropriate for our high-metallicity clouds:  $r = R$  and  $t = t_{\text{exp}}$ . Note that in that case  $\dot{\rho}_* \propto R^{-1}$ . Comparing to the observed, global star formation density,  $\dot{\rho}_* \approx 0.1 M_{\odot} \text{ Mpc}^{-3} \text{ yr}^{-1}$  (e.g., Fardal et al. 2006), we see that for the high-metallicity clouds to be supernova remnants, essentially all star formation should be intergalactic, which of course is highly unlikely.

If the high-metallicity clouds are intergalactic planetary nebulae, then we can use the same calculation, provided we adjust  $M_{100}$ , and interpret  $\dot{\rho}_*$  as averaged over the range of lifetimes of the progenitor stars. Since we now have  $M_{100} \ll 1$ , this scenario can probably not be ruled out on this basis.

#### 6.4.3 Evolution of individual clouds

If the clouds are short-lived, as we argued is likely, it is interesting to ask what they look like at different points in their lifetimes. Figure 24 shows how the column densities of a number of potentially observable ions vary as a function of the density/ionization parameter. We assumed a path length equivalent to that of a sightline passing through the center of a spherical, constant density gas cloud with mass  $M_g = 10^2 M_{\odot}$ . The cloud has solar abundances, a constant temperature of  $10^4 \text{ K}$ , and is exposed to the model of the  $z = 2.3$  metagalactic radiation field of Haardt & Madau (2001) from galaxies and quasars. Provided self-shielding is unimportant, which is true for  $N_{\text{HI}} < 10^{17} \text{ cm}^{-2}$ , all curves can be shifted vertically in proportion with  $M^{1/3}$  and in proportion to the elemental abundances.

Figure 24 shows that unless the clouds are much more massive than  $10^2 M_{\odot}$  or much more metal-rich than the sun, they would be undetectable for  $n_{\text{H}} \ll 10^{-4} \text{ cm}^{-3}$  ( $U \gg 10^{-1}$ ). Thus, if our clouds were to expand by more than a factor of a few, we would no longer be able to detect them. The CIV line remains detectable up to much higher densities,  $n_{\text{H}} \lesssim 10^{-1} \text{ cm}^{-3}$ , but for  $n_{\text{H}} \gtrsim 10^{-3} \text{ cm}^{-3}$  NV and particularly OVI would typically be swamped by contamination and noise. For high-density absorbers we predict  $N_{\text{CIV}} \ll N_{\text{HI}}$ , which means that we would only be able to recognize them as high-metallicity clouds if we knew they had high densities. Since we would not know this (because our upper limits on the columns of NV and OVI would exceed the true values), clouds with  $n_{\text{H}} \gtrsim 10^{-3} \text{ cm}^{-3}$  will not be included in our sample.

<sup>10</sup> Models of shells driven by winds have been invoked to explain other classes of absorbers. These models usually assume a hot wind fluid within a spherical, unfragmented shell. We believe that such an idealized model is inconsistent with both observations and simulations of galactic winds in a realistic context, which predict a clumpy fluid and anisotropic outflows.

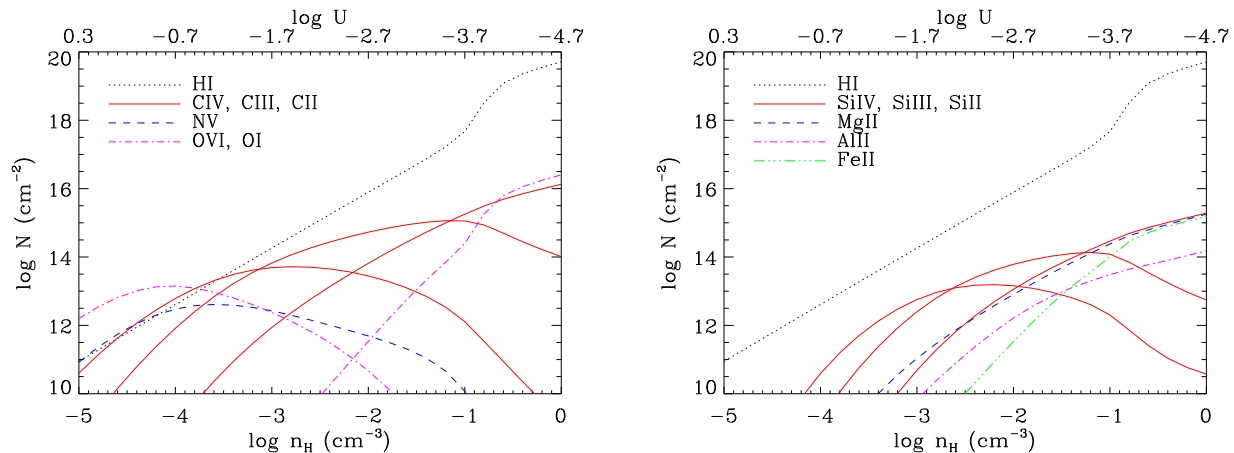


**Figure 24.** Column densities of various ions as a functions of density (lower  $x$ -axis) and ionization parameter (upper  $x$ -axis) for a sight line through the center of a spherical  $10^2 M_{\odot}$  gas cloud. The cloud was assumed to have a constant density, a temperature of  $10^4$  K, and solar abundances. We used the Haardt & Madau (2001) model for the integrated  $z = 2.3$  UV/X-ray background from galaxies and quasars.

## 6.5 Comparison with other observations

### 6.5.1 Weak MgII absorbers

Clouds with densities much higher than the clouds in our sample can be detected in low-ionization lines (see Fig. 24). The Mg II ( $\lambda\lambda$  2796, 2803) doublet is a particularly effective tracer because it is strong, does not suffer from contamination by Lyman series lines, and is easily identifiable. Its disadvantage is that because of its large rest wavelength, studies in the optical are only possible for  $z \sim 1$ , in which case space-based UV-spectroscopy is required to measure hydrogen column densities (without which metallicities and sizes cannot be determined) as well as to measure most other metal lines (which are required to constrain the ionization parameter).

Rigby et al. (2002) find that at  $z \lesssim 1$ , single-cloud, weak (equivalent width  $< 0.3 \text{ \AA}$ ) Mg II absorbers are metal-rich ( $Z > 0.1 Z_{\odot}$ ) and that at least the subset of systems for which Fe II is detected must be compact ( $R \sim 10$  pc). Rigby et al. estimate that the weak Mg II clouds with iron detections have densities  $n_{\text{H}} \sim 10^{-1} \text{ cm}^{-3}$ , assuming that they are irradiated by the integrated UV radiation from quasars as modeled for  $z = 1$  by Haardt & Madau (1996). This gives a typical cloud mass of order  $10 M_{\odot}$ , which is similar to that of our high-metallicity sample and is thus suggestive of a connection between the two types of clouds.

Rigby et al. (2002) estimate a rate of incidence of  $dN/dz \approx 0.25$  for the subset of weak Mg II systems showing Fe II absorption. Assuming  $(\Omega_m, \Omega_{\Lambda}, h) = (0.3, 0.7, 0.7)$  and  $z = 1$  we find from equation (12) a comoving number density of  $n \sim 8 \times 10^4 \text{ Mpc}^{-3} (R/10 \text{ pc})^{-2}$ . This is only about a factor 5 greater than our high-metallicity systems at  $z = 2.3$  [equation (13)], which is remarkably close, particularly if we take into account the substantial uncertainties in both of these estimates. One might expect the number densities of the two types of absorbers to be similar if each cloud contained both a low and a high-ionization phase (e.g., in a core-halo structure). However, although one would expect high density peaks giving rise to low-ionization lines to be surrounded by more dilute, highly ionized gas, it would seem

natural to also have a population of gas clouds with central densities that are too low to give rise to low-ionization lines. Moreover, even if every high-metallicity cloud contained a weak Mg II core, there is no obvious reason why the two phases should contain similar masses.

The mass coincidence could be accounted for if the high-metallicity clouds were created as little dense knots, for example through hydrodynamic and/or thermal instabilities in a high-pressure environment, which then expanded to become weak Mg II, and later high-metallicity CIV, clouds on timescales that are short compared with the Hubble time (and thus with the difference in age between the  $z = 1$  and  $z = 2.3$  universe). However, there is no reason why the lifetimes of the Mg II and CIV phases should be similar, as would need to be the case for their number densities to agree. On the other hand, given that that the two number densities were determined for different redshifts and that the rates of incidence and cloud sizes are highly uncertain, it would be surprising if the number densities agreed even if the CIV and weak Mg II and timescales were identical.

### 6.5.2 OVI systems

Simcoe et al. (2006) used ionization models and a range of low- and high-ionization lines to determine the properties of strong O VI systems within 100–200 kpc from starbursting galaxies at  $z \approx 2.5$ . They found typical densities  $n_{\text{H}} \gtrsim 10^{-3} \text{ cm}^{-3}$ , sizes  $R \sim 10^2 - 10^4$  pc and metallicities  $Z \sim 10^{-2} - 10^0 Z_{\odot}$ . The systems selected by Simcoe et al. tend to have very strongly saturated HI absorption which should mean that most of their sizes are in fact upper limits and most of their metallicities lower limits. Their selection criteria appear to result in a sample of clouds with a range of physical properties, but their results clearly show that there exist compact, metal-rich clouds in the vicinity of galaxies.

Bergeron & Herbert-Fort (2005) also found a range of properties for O VI absorbers at this redshift, including a subset of metal-rich clouds. Like Carswell et al. (2002) and the present study, they found that the high-metallicity clouds cannot be self-gravitating. Bergeron &

Herbert-Fort (2005) also showed that the majority of metal-rich O VI clouds are within  $500 \text{ km s}^{-1}$  of strong HI absorption ( $\tau_{\text{Ly}\alpha} > 4$ ) and that at least half of their O VI lines are too narrow for collisional ionization to be effective.

### 6.5.3 HI 21 cm emitters in the halo of the Galaxy

If we increase the cloud density above that of the weak Mg II systems, the Mg II lines would become too strong to be included in Rigby et al.’s sample of “weak” lines. Figure 24 shows that the clouds would be Lyman limit systems (i.e.,  $N_{\text{HI}} > 10^{17} \text{ cm}^{-2}$ ) with strong C II, O I, Mg II, Al II, Si II, and Fe II absorption. However, given their small cross sections, the rate of incidence would be extremely small if the number density of such systems were similar to that of the high-metallicity CIV clouds and one would require a very large sample of quasars to see just a few.

If such a population of compact, metal-rich Lyman limit absorbers were present in the halo of our own galaxy, its 21 cm emission might be detectable. Interestingly, Lockman (2002) recently discovered that as much as half of the HI in the inner Galaxy’s halo is made up of tiny clouds with  $N_{\text{HI}} \sim 10^{19} \text{ cm}^{-2}$ ,  $R \sim 10 \text{ pc}$ ,  $n_{\text{H}} \sim 10^{-1} - 1 \text{ cm}^{-3}$ , and  $M \sim 10 - 10^2 M_{\odot}$ . Such clouds may correspond to high-velocity Ca II absorbers (Richter et al. 2005). Unfortunately, metallicities are not available for any of the clouds. Regardless of the metal content of the clouds, this observation does show that galaxies are capable of forming large numbers of compact gas clouds in the mass range of the weak Mg II and high-metallicity CIV clouds.

### 6.5.4 Direct constraints on cloud sizes

Observations of gravitationally lensed quasars confirm the small sizes of low-ionization clouds derived from ionization modeling. Rauch, Sargent, & Barlow (1999) found a low-ionization (C II, O I, and Si II) absorber with a size  $\sim 10 \text{ pc}$  and solar metallicity. Several studies have shown that while Mg II complexes are larger than about 0.5 kpc, individual Mg II clouds cannot be traced over distances  $\gg 10^2 \text{ pc}$  (e.g., Petitjean et al. 2000; Rauch et al. 2002; Churchill et al. 2004; Ellison et al. 2004).

Intriguingly, Hao et al. (2006) recently found that a  $z = 1.48$  system with strong Mg II and Fe II absorption, observed towards a  $z = 4.05$  Gamma-Ray Burst (GRB), showed strong variability over timescales of days. They found that this implies absorber sizes similar to the GRB beam size,  $\sim 10^{-2} \text{ pc}$ . Such small sizes had been predicted by Frank et al. (2006) because they could explain the different rates of incidence of strong Mg II absorption in sight lines towards quasars and GRBs (Prochter et al. 2006).

Tzanavaris & Carswell (2003) used evidence for partial coverage of  $z \approx 3$  CIV components in the spectrum of one quasar to infer a lower limit on the size of<sup>11</sup> 150 pc and a most likely size  $R \sim 1 \text{ kpc}$ . The study of Rauch, Sargent, & Barlow (2001), who analyzed CIV coincidences in three

gravitationally lensed quasar pairs at  $z \sim 2-3$ , is most relevant for us. Their figures 8 and 9 show that the fractional difference in the CIV columns of *single components* (but not complexes<sup>12</sup>) increases sharply from  $\lesssim 10\%$  for separations less than 30 pc to 20–90% for separations above 50 pc. They find that if the redshift of the lens of one of the quasars is 1.32 rather than 0.73, then the transition would be shifted to about 100 pc.

Thus, it appears that CIV clouds (with  $N_{\text{CIV}} \gtrsim 10^{13} \text{ cm}^{-2}$ ) have characteristic sizes  $R \sim 10^2 - 10^3 \text{ pc}$ , which agrees remarkably well with the median upper limit on the size we inferred for our high-metallicity clouds ( $R \lesssim 10^3 \text{ pc}$ ), but is slightly greater than our preferred size ( $R \sim 10^2 \text{ pc}$ ). Note that for 6 out of 28 clouds, our robust and conservative upper limits are  $R < 10^{2.5} \text{ pc}$ . On the other hand, the 5 clouds with the weakest limits on the density all have upper limits greater than  $10^4 \text{ pc}$ . If there is scatter in the sizes, which seems natural, then our selection criteria for high-metallicity will preferentially pick out small clouds. This is because the inferred limits on the metallicity and size scale as  $Z \propto N_{\text{HI}}^{-1} \propto R^{-1}$ .

If the clouds are expanding, then we predict higher density clouds (i.e., clouds with lower ionization) to be smaller and clouds with lower densities (which would be difficult to detect in CIV but may still be visible in O VI) to be larger. Such a trend is consistent with our data (see Fig. 6), with sizes inferred from quasar pairs, and with ionization models of other populations.

## 6.6 Implications for the mixing of metals

We argued that our high-metallicity clouds are likely short-lived and that they were probably born with high densities. What will be their ultimate fate? Presumably, they will expand until they reach pressure equilibrium with their environment. If that environment is the diffuse IGM, then it will have the same temperature as the clouds,  $T \sim 10^4 \text{ K}$ . Pressure equilibrium then implies that the densities would also be the same. At that point, the term cloud would be somewhat of a misnomer, “metal concentration” might better describe the situation.

When the cloud is done expanding, its HI column density will be much smaller than that associated with the environment. To see this, note that when we observe the clouds, their densities are about 1.5 dex higher than the cosmic mean. They will thus typically have to increase in size by 0.5 dex to reach pressure equilibrium with their environment, or less if the latter is overdense. At that point they will still be much smaller than typical, moderately overdense HI clouds, which are observed to have sizes  $R \sim 10^2 \text{ kpc}$  (e.g., Bechtold et al. 1994). Since their densities and temperatures are now the same as those of the environment, so will their HI

<sup>11</sup> Tzanavaris & Carswell (2003) overestimated the sizes by a factor of 2 due to an error, see Ellison et al. (2004). We quote the correct results here.

<sup>12</sup> There are other studies of CIV absorption in quasar pairs that looked at complexes (e.g., Ellison et al. 2004), but we have not found any other studies that also looked at differences between individual clouds. Clearly, only individual components can be compared with the cloud sizes inferred from our ionization models.

densities. Thus,  $N_{\text{HI}} = n_{\text{HI}}R$  will be much greater for the environment than for the clouds.

Another way to see this goes as follows. Unless the environment is underdense, the hydrodynamical timescales are short enough that its density will fluctuate on the local Jeans scale (Schaye 2001). Hence, the HI column associated with the environment will typically be  $N_{\text{HI}} \sim n_{\text{HI}}L_J(n_{\text{H}}, T)$ , which is much greater than the HI column associated with the high-metallicity gas because we found that the clouds have  $R \ll L_J$  (note that if  $R < L_J$  initially, then expansion at fixed temperature will not change this because [see equations (7) and (9)]  $R/L_J \propto n_{\text{H}}^{-1/3}/n_{\text{H}}^{-1/2} \propto n_{\text{H}}^{1/6}$ ).

If the HI column associated with the environment is much greater than that associated with the metals, then we would no longer consider the cloud to be a high-metallicity system. If the high-metallicity gas is at rest with respect to its environment, then we would not be able to tell whether the metals are mixed throughout the HI cloud or not, except through observations that can probe the sizes of the metal-containing gas directly, such as those comparing quasar pairs.

Thus, we can only recognize a cloud as having high-metallicity as long as it is denser than its environment. The density at which a metal-rich cloud will stop expanding, will vary according to the density of its environment. After it has reached pressure equilibrium, it will look like an ordinary, low-metallicity absorption system. This suggests that the metals in ordinary systems may also be concentrated in patches that are very small compared to the HI coherence length.

In fact, clouds in high-density, photo-ionized environments would look like ordinary metal systems even while they are still expanding. From our data we can only tell that the metallicity is high when their C IV/HI fraction is close to maximum (see §6.4.3). Clouds that end up in higher density environments presumably also exist, but would at no point in their evolution be included in our sample.

As we discussed in §6.5.4, direct observations of the sizes of individual metal-line clouds, including C IV, typically find very small sizes. Significantly, these observations do not attempt to select high-metallicity gas, except for the unavoidable condition that the metal line be detectable. This suggests that intergalactic metals generally reside in small patches of gas. The metallicity we infer from absorption studies is then not determined by the abundances of heavy elements on the size of the metal concentrations, but by the metallicity smoothed over the size of the HI absorber, which is well known to be much greater.

We are therefore inclined to conclude that the intergalactic metals are transported from galaxies in the form of dense, high-metallicity clouds. This is also supported by the large amount of metals that may have passed through the high-metallicity cloud phase [equation (29)]. Although the clouds expand until they become part of the IGM, the metals remain poorly mixed on scales greater than  $10^3$  pc for very low overdensities and on even smaller scales for higher densities.

This scenario has some profound implications. When smoothed on small scales ( $\ll$  kpc), most of the IGM (which contains most of the baryons in the universe) may be of primordial composition. A very small amount of intergalactic gas is, however, metal-rich. Such pockets of metal-rich mate-

rial will cool more efficiently, which may change the physics of galaxy formation. The number of metal-line components per HI absorber depends on the number of metal concentrations along the line of sight. The absence of associated absorption by heavy elements, even in a spectrum with an infinite signal-to-noise ratio, does not necessarily imply that the HI absorber is metal-free.

## 7 SUMMARY AND CONCLUSIONS

We performed a search for high-metallicity C IV absorption in 9 high-quality spectra of  $2.2 < z < 3.3$  quasars taken with the UVES spectrograph at the VLT telescope. We used a novel approach to robustly select high-metallicity absorbers. First all C IV absorbers were identified and decomposed into Voigt profiles using VPFIT. We then used a new algorithm to automatically measure conservative upper limits on the column densities of associated transitions. The resulting lower limits on  $N_{\text{CIV}}/N_{\text{HI}}$  together with the maximum predicted C IV/HI fraction, were used to set lower limits on the metallicity and to select 26 C IV components with  $[\text{C}/\text{H}] > -1$ . Two additional clouds were determined to have  $[\text{C}/\text{H}] > -1$  after observed lower limits on the density, obtained from the observed lower limits on  $N_{\text{CIV}}/N_{\text{NV}}$  and  $N_{\text{CIV}}/N_{\text{OVI}}$ , were taken into account. Due to our reliance on upper limits, both our sample selection and the physical properties inferred from our ionization model are robust with respect to line blending, noise, contamination, and the presence of phases other than the one responsible for the C IV absorption.

In total we selected 28 high-metallicity components in 12 different systems, giving rates of incidence of  $dN/dz > 7 \pm 1$  and  $> 3.0 \pm 0.9$  for components and systems, respectively. The mean system redshift is 2.25 and the redshift below which half of the redshift path searched is located is 2.24. Like the general population of C IV absorbers, some of the clouds appear isolated, others are not. Some are close to strong HI systems, others are not. The high-metallicity clouds have median C IV column density  $\log[N_{\text{CIV}}(\text{cm}^{-2})] = 13.0$ . The upper limits on  $N_{\text{NV}}$  and  $N_{\text{OVI}}$  are similar to those for the general population of C IV clouds, but the C IV/HI ratio is (by selection) much higher ( $\log(N_{\text{CIV}}/N_{\text{HI}}) > -0.8$ ).

We find no evidence for clustering around the redshift of the quasar<sup>13</sup>. Combined with the narrow line widths (typically  $b_{\text{CIV}} < 10 \text{ km s}^{-1}$ ) and the absence of evidence for partial coverage, this strongly suggests that the clouds are intervening rather than ejected.

Assuming that the clouds are irradiated by the intergalactic radiation field from quasars and galaxies as modeled by Haardt & Madau (2001) for  $z = 2.3$  and that they have temperatures  $T = 10^4$  K, we derived lower limits on the density by comparing an ionization model to the measured lower limits on the ratios  $N_{\text{CIV}}/N_{\text{NV}}$  and  $N_{\text{CIV}}/N_{\text{OVI}}$ . Similarly, for the 15 clouds for which our spectra covered the associated C III, we used the upper limits on  $N_{\text{CIII}}/N_{\text{CIV}}$  and  $N_{\text{SiIV}}/N_{\text{CIV}}$  to obtain upper limits on the density and the abundance of silicon relative to carbon, respectively.

<sup>13</sup> Regions closer than 4,000  $\text{km s}^{-1}$  to the quasar were excluded.

The lower and upper limits on the density are consistent in all cases. The median limits are  $[C/H] > -0.42$ ,  $\log[n_H \text{ (cm}^{-3}\text{)}] > -4.0$ ,  $\log[R \text{ (pc)}] < 3.2$ , and  $[Si/C] < 1.5$ . There is considerable scatter around the medians, with evidence for anti-correlations between the limits on size and density as well as between metallicity and size, but these trends may be caused by selection effects. The median upper limit on the density is  $\log[n_H \text{ (cm}^{-3}\text{)}] < -3.0$ , which suggests a typical value  $n_H \sim 10^{-3.5} \text{ cm}^{-2}$ , about 50 times the mean density at  $z = 2.25$ . Using this density rather than the median lower limit yields  $R \sim 10^2 \text{ pc}$  and a gas mass  $M_g \sim 10^2 M_\odot$ .

The high rate of incidence suggest that local sources do not dominate the ionizing radiation field. Both the distribution of the clouds in the CIV/OVI-CIV/NV plane and the line widths suggest that collisional ionization is unimportant. In any case, the conclusions that the clouds are compact and metal-rich would be strengthened if (a) the clouds were exposed to a radiation field that is harder and/or more intense than the Haardt & Madau (2001) model; (b) the gas was hot enough for collisional ionization to be important; (c) oxygen were overabundant relative to carbon; (d) the metals were more highly ionized than they would be in photo-ionization equilibrium.

The high-metallicity clouds are far too small (relative to their densities) to be self-gravitating. For the clouds to be gravitationally confined, their gas fraction would need to be completely negligible, with dark matter (or stellar) masses of order  $10^6 - 10^7 M_\odot$ . Dark matter minihalos collapsing at  $z \sim 10$  would have virial radii similar to the cloud sizes and would lose their gas content during reionization (or earlier due to feedback from star formation), but the predicted halo number densities are too small to account for a significant fraction of the high-metallicity clouds.

If the clouds are confined by an external medium, then this medium needs to have the same (low) pressure and it must not give rise to HI absorption that is stronger than allowed by the observations. We found that if the medium is self-gravitating, this implies a temperature  $T > 10^5 \text{ K}$  and a density not much higher than the cosmic mean. Higher densities are, however, possible if the confining medium is expanding.

If the clouds are unconfined, then their natural lifetime is the timescale for free expansion, which is only  $\sim 10^7 \text{ yr}$ . If there is a confining medium, then hydrodynamical instabilities would still limit the lifetime of the clouds to similar values, unless they move through the medium with velocities  $\ll 10 \text{ km s}^{-1}$ .

If the clouds are short-lived, they will have been denser in the past. If we decrease their size by factor of a few, they will look like weak Mg II clouds (e.g., Rigby et al. 2002). If we again compress them by a factor of a few, they will look like the HI clouds discovered by Lockman (2002) in the halo of our Galaxy. On the other hand, if we let them expand by a factor of a few, they will become undetectable in CIV.

Given their small cross sections, the clouds must be extremely numerous for us to see as many as we do. We estimate a comoving number density of order  $10^4 \text{ Mpc}^{-3}$  which exceeds that of observable galaxies (down to  $0.1 L_*$ ) by about a factor of  $10^6$ . If the clouds were to reside in halos centered on such galaxies, then we would require halo radii of order  $10^2 \text{ kpc}$  (for a cloud covering factor of order unity).

If the clouds were formed close to the galaxy, it would take them  $10^9 \text{ yr}$  to reach  $10^2 \text{ kpc}$  if they traveled at  $10^2 \text{ km s}^{-1}$ , a typical speed for superwinds. Since this is much greater than the characteristic lifetime of the clouds, for the clouds to originate in winds, they would need to be continuously formed and destroyed. This is expected in a galactic wind, where swept up shells fragment due to thermal and hydrodynamical instabilities. Observations of local starburst galaxies indeed reveal a clumpy medium embedded in an (initially) hot fluid.

There are other possibilities, besides galactic winds, for the origin of the clouds. Most have already been discussed in the context of other populations of metal-rich, compact clouds, such as weak Mg II and strong OVI absorbers. At least one scenario, intergalactic supernovae remnants, can be ruled out if the clouds are short-lived because it would imply that most star formation would be intergalactic.

The high-metallicity clouds contain only a negligible fraction of the baryons and about an order of magnitude less carbon than can be traced by CIV in the diffuse IGM. However, if they are short-lived, then the amount of metal that has passed through this phase would be greater than the amount contained in the clouds at a given time by a factor of order  $t_H/t$ . Although gas can be cycled through clouds multiple times and although many of the clouds may end up in galaxies, this does suggest that all of the metals in the diffuse IGM may at one point have been contained in compact, metal-rich clouds.

When the clouds reach pressure equilibrium with the diffuse, photo-ionized IGM, they will still have sizes that are more than an order of magnitude smaller than those of the diffuse HI clouds, which are known to be of order  $10^2 \text{ kpc}$ . At that point the HI column of the confining medium will completely wash out the HI associated with the metal concentration and the cloud will look like an ordinary, low-metallicity absorber. In fact, even high-metallicity CIV clouds that are still expanding will look like ordinary metal-line systems until their densities are low enough for the CIV/HI fraction to be close to its maximum.

This suggests that all intergalactic metals may reside in small patches of highly-enriched gas. This scenario is supported by independent constraints, such as those obtained from observations of metal-line anti-coincidences and partial covering in the images of gravitationally lensed quasars. We are therefore inclined to conclude that metals are transported into the IGM in the form of dense, high-metallicity clouds. These clouds expand as they move out, until they end up at rest and in pressure equilibrium with the IGM, but at that point they still fill only a very small fraction of the volume.

Thus, most of the IGM, and therefore the baryons in the universe, may be of primordial composition. This is not inconsistent with previous work on the distribution of metals in the IGM, because those studies implicitly smooth the gas on the scale of the HI absorbers. It does mean, however, that much of the scatter in the metallicity found in studies of quasar absorption spectra may be due to scatter in the number of metal-rich patches intersected by the line of sight, rather than by scatter in the metallicity on the scale of the HI absorbers. In particular, the absence of metal-line absorption associated with an HI line, even in a spectrum

with an infinite signal-to-noise ratio, does not necessarily mean the HI absorber contains no metals.

Poor small-scale mixing of metals not only requires a re-interpretation of previous observational analyses, it may also affect the physics of the IGM and the formation of galaxies. For example, the cooling rates depend on local abundances, rather than the metallicity obtained after smoothing over  $\sim 10^2$  kpc.

## ACKNOWLEDGMENTS

We are grateful to the ESO Archive, without their help this work would not have been possible. We would also like to thank the referee, Rob Simcoe, for a helpful report. JS gratefully acknowledges support from Marie Curie Excellence Grant MEXT-CT-2004-014112.

## REFERENCES

- Adelberger, K. L., Steidel, C. C., Shapley, A. E., & Pettini, M. 2003, *ApJ*, 584, 45
- Adelberger, K. L., Shapley, A. E., Steidel, C. C., Pettini, M., Erb, D. K., & Reddy, N. A. 2005, *ApJ*, 629, 636
- Aguirre, A., Hernquist, L., Schaye, J., Weinberg, D. H., Katz, N., & Gardner, J. 2001, *ApJ*, 560, 599
- Aguirre, A., Schaye, J., Kim, T., Theuns, T., Rauch, M., & Sargent, W. L. W. 2004, *ApJ*, 602, 38
- Aracil, B., Tripp, T. M., Bowen, D. V., Prochaska, J. X., Chen, H.-W., & Frye, B. L. 2006, *MNRAS*, 367, 139
- Bechtold, J., Crotts, A. P. S., Duncan, R. C., & Fang, Y. 1994, *ApJL*, 437, L83
- Bergeron, J., Aracil, B., Petitjean, P., & Pichon, C. 2002, *A&A*, 396, L11
- Bergeron, J., & Herbert-Fort, S. 2005, *ArXiv Astrophysics e-prints*, arXiv:astro-ph/0506700
- Carswell, B., Schaye, J., & Kim, T. 2002, *ApJ*, 578, 43
- Charlton, J. C., Ding, J., Zonak, S. G., Churchill, C. W., Bond, N. A., & Rigby, J. R. 2003, *ApJ*, 589, 111
- Chen, H.-W., Lanzetta, K. M., & Webb, J. K. 2001, *ApJ*, 556, 158
- Churchill, C. W., Mellon, R. R., Charlton, J. C., & Vogt, S. S. 2003, *ApJ*, 593, 203
- Dedikov, S. Y., & Shchekinov, Y. A. 2004, *Astronomy Reports*, 48, 9
- D’Odorico, S., Cristiani, S., Dekker, H., Hill, V., Kaufer, A., Kim, T., & Primas, F. 2000, *SPIE*, 4005, 121
- Ellison, S. L., Ibata, R., Pettini, M., Lewis, G. F., Aracil, B., Petitjean, P., & Srianand, R. 2004, *A&A*, 414, 79
- Fardal, M. A., Katz, N., Weinberg, D. H., & Dav’e, R. 2006, *ArXiv Astrophysics e-prints*, arXiv:astro-ph/0604534
- Ferland, G. J. 2000, *Revista Mexicana de Astronomia y Astrofisica Conference Series*, 9, 153
- Ferland, G. J., Korista, K. T., Verner, D. A., Ferguson, J. W., Kingdon, J. B., & Verner, E. M. 1998, *PASP*, 110, 761
- Frank, S., Bentz, M. C., Stanek, K. Z., Dietrich, M., Kochanek, C. S., Mathur, S., & Peterson, B. M. 2006, *ArXiv Astrophysics e-prints*, arXiv:astro-ph/0605676
- Furlanetto, S. R., Schaye, J., Springel, V., & Hernquist, L. 2004, *ApJ*, 606, 221
- Gregori, G., Miniati, F., Ryu, D., & Jones, T. W. 1999, *ApJL*, 527, L113
- Haardt, F., & Madau, P. 1996, *ApJ*, 461, 20
- Haardt, F., & Madau, P. 2001, to be published in the proceedings of XXXVI Rencontres de Moriond, astro-ph/0106018
- Hamann, F., Barlow, T. A., Junkkarinen, V., & Burbidge, E. M. 1997, *ApJ*, 478, 80
- Hao, H., et al. 2006, *ArXiv Astrophysics e-prints*, arXiv:astro-ph/0612409
- Heckman, T. M., Lehnert, M. D., Strickland, D. K., & Armus, L. 2000, *ApJS*, 129, 493
- Jones, T. W., Kang, H., & Tregillis, I. L. 1994, *ApJ*, 432, 194
- Keeney, B. A., Stocke, J. T., Rosenberg, J. L., Tumlinson, J., & York, D. G. 2006, *AJ*, 132, 2496
- Kim, T.-S., Carswell, R. F., Cristiani, S., D’Odorico, S., & Giallongo, E. 2002, *MNRAS*, 335, 555
- Lockman, F. J. 2002, *ApJL*, 580, L47
- Mac Low, M., McKee, C. F., Klein, R. I., Stone, J. M., & Norman, M. L. 1994, *ApJ*, 433, 757
- Mac Low, M. & Ferrara, A. 1999, *ApJ*, 513, 142
- Martin, C. L., Kobulnicky, H. A., & Heckman, T. M. 2002, *ApJ*, 574, 663
- Milutinović, N., Rigby, J. R., Masiero, J. R., Lynch, R. S., Palma, C., & Charlton, J. C. 2006, *ApJ*, 641, 190
- Miralda-Escudé, J. 2005, *ApJL*, 620, L91
- Misawa, T., Charlton, J. C., Eracleous, M., Ganguly, R., Tytler, D., Kirkman, D., Suzuki, N., & Lubin, D. 2007, *ArXiv Astrophysics e-prints*, arXiv:astro-ph/0702101
- Norman, C. A., Bowen, D. V., Heckman, T., Blades, C., & Danly, L. 1996, *ApJ*, 472, 73
- Péroux, C., Dessauges-Zavadsky, M., D’Odorico, S., Sun Kim, T., & McMahon, R. G. 2005, *MNRAS*, 363, 479
- Péroux, C., Meiring, J. D., Kulkarni, V. P., Ferlet, R., Khare, P., Lauroesch, J. T., Vladilo, G., & York, D. G. 2006, *MNRAS*, 372, 369
- Petitjean, P., Aracil, B., Srianand, R., & Ibata, R. 2000, *A&A*, 359, 457
- Pettini, M., Kellogg, M., Steidel, C. C., Dickinson, M., Adelberger, K. L., & Giavalisco, M. 1998, *ApJ*, 508, 539
- Pieri, M. M., Schaye, J., & Aguirre, A. 2006, *ApJ*, 638, 45
- Prochaska, J. X., O’Meara, J. M., Herbert-Fort, S., Burles, S., Prochter, G. E., & Bernstein, R. A. 2006, *ApJL*, 648, L97
- Prochter, G. E., et al. 2006, *ApJL*, 648, L93
- Rauch, M., Carswell, R. F., Chaffee, F. H., Foltz, C. B., Webb, J. K., Weymann, R. J., Bechtold, J., & Green, R. F. 1992, *ApJ*, 390, 387
- Rauch, M., Sargent, W. L. W., & Barlow, T. A. 1999, *ApJ*, 515, 500
- Rauch, M., Sargent, W. L. W., & Barlow, T. A. 2001, *ApJ*, 554, 823
- Rauch, M., Sargent, W. L. W., Barlow, T. A., & Simcoe, R. A. 2002, *ApJ*, 576, 45
- Reed, D. S., Bower, R., Frenk, C. S., Jenkins, A., & Theuns, T. 2007, *MNRAS*, 374, 2
- Richter, P., Westmeier, T., & Brüns, C. 2005, *A&A*, 442, L49
- Rigby, J. R., Charlton, J. C., & Churchill, C. W. 2002, *ApJ*, 565, 743
- Schaye, J. 2001, *ApJ*, 559, 507
- Schaye, J., Aguirre, A., Kim, T., Theuns, T., Rauch, M., & Sargent, W. L. W. 2003, *ApJ*, 596, 768 (S03)
- Schaye, J., & Aguirre, A. 2005, *IAU Symposium*, 228, 557
- Schaye, J. 2006, *ApJ*, 643, 59
- Shelton, R. L. 1998, *ApJ*, 504, 785
- Simcoe, R. A., Sargent, W. L. W., & Rauch, M. 2004, *ApJ*, 606, 92
- Simcoe, R. A., Sargent, W. L. W., Rauch, M., & Becker, G. 2006, *ApJ*, 637, 648
- Spergel, D. N. et al. 2003, *ApJS*, 148, 175
- Steidel, C. C., Adelberger, K. L., Giavalisco, M., Dickinson, M., & Pettini, M. 1999, *ApJ*, 519, 1
- Stocke, J. T., Penton, S. V., Danforth, C. W., Shull, J. M., Tumlinson, J., & McLin, K. M. 2006, *ApJ*, 641, 217
- Telfer, R. C., Kriss, G. A., Zheng, W., Davidsen, A. F., & Tytler,

D. 2002, ApJ, 579, 500  
 Tripp, T. M. et al. 2002, ApJ, 575, 697  
 Tripp, T. M., Aracil, B., Bowen, D. V., & Jenkins, E. B. 2006, ApJL, 643, L77  
 Tzanavaris, P., & Carswell, R. F. 2003, MNRAS, 340, 937  
 Veilleux, S., Cecil, G., & Bland-Hawthorn, J. 2005, ARA&A, 43, 769  
 Webb, J. K. 1987, Ph.D. Thesis, Univ. Cambridge

$\log N < 13.5$ , and double this for higher values. The quantities given in Table 3 reflect this choice.

This paper has been typeset from a  $\text{\TeX}/\text{\LaTeX}$  file prepared by the author.

### APPENDIX A: COLUMN DENSITY UPPER LIMITS

If the redshift and Doppler parameter are determined for some reference ion, for example CIV, then for other ions within the same region the redshift will be the same and one can estimate a range of acceptable Doppler parameters  $b$  under the assumption that there is a turbulent component  $b_{\text{turb}}$  which is the same for all ions and a thermal component  $b_{\text{T}}$  which is proportional to the square root of the mass  $m$  of the ion. Then the two components add in quadrature to give the actual Doppler parameter, so

$$b^2 = b_{\text{turb}}^2 + b_{\text{T}}^2.$$

where  $b_{\text{T}} = \sqrt{\frac{m}{m_{\text{ref}}}} b_{\text{T,ref}}$  where the subscript 'ref' is the value for the reference ion. Possible extreme values for  $b$  are then determined assuming that the Doppler parameter for the reference ion is fully turbulent and fully thermal. In the implementation used here this range was extended by using the  $1\text{-}\sigma$  error estimates for the reference ion, so reference Doppler parameters  $b_{\text{ref}} \pm \sigma$  were used and the most extreme values of  $b$  adopted to give the Doppler parameter ranges for each ion.

Using the redshift for the reference ion, and a sequence of Doppler parameters from the minimum to maximum obtained in this way, a grid of Voigt profiles convolved with the instrument profile was constructed for the transitions of the test ion available in the observed range. For Lyman lines these could, in principle, be several of the Lyman series, but for the application here generally only  $\text{Ly}\alpha$  and  $\text{Ly}\beta$  were used since they are covered for most of the sample. The line profiles were compared with the data, and a  $\chi^2$  determined for pixels where the Voigt profile was below the data value plus  $1\text{-}\sigma$ , and within  $2b$  of the line center for each transition. If no pixels satisfied this criterion then the column density was increased until some did. The column density limit for each  $b$ -value was taken as the highest value for which the  $\chi^2$  value over this range had a probability of occurring by chance of less than 0.16 (corresponding to a  $1\text{-}\sigma$  one-sided deviation). The final overall limit adopted was the maximum of these over the range of Doppler parameters. This yields a maximum possible column density for the ion even in the presence of blends, since it is effectively only the pixels where the trial fitted profile is too low which contribute to the significance level.

The chance probability criterion for accepting or rejecting possible line profiles is arbitrary, so there seemed little point in iterating or interpolating to achieve high accuracy. We adopted a column density step of  $\Delta \log N = 0.05$  for

**Table 3.** High-metallicity components

QSO (1)	$z$ (2)	$\log N_{\text{HI}}$ (3)	$\log N_{\text{CIII}}$ (4)	$\log N_{\text{CIV}}$ (5)	Error (6)	$\log N_{\text{NV}}$ (7)	$\log N_{\text{OVI}}$ (8)	$\log N_{\text{SiIII}}$ (9)	$\log N_{\text{SiIV}}$ (10)	$b_{\text{CIV}}$ (11)	Error (12)
Q0122–380	2.062560	< 13.050		12.932	0.039	< 12.900	< 13.600	< 12.150	< 12.100	17.90	5.10
HE0151–4326	2.415724	< 13.400	< 13.100	12.954	0.031	< 12.250	< 14.400	< 11.050	< 11.400	17.20	2.70
HE0151–4326	2.419671	< 12.950	< 12.800	12.747	0.009	< 13.350	< 12.850	< 11.150	< 11.600	7.20	0.90
HE0151–4326	2.468097	< 12.850	< 12.650	12.970	0.008	< 12.850	< 13.800	< 11.050	< 11.400	12.20	0.50
HE0151–4326	2.468720	< 13.050	< 13.000	12.628	0.225	< 12.800	< 13.500	< 11.100	< 11.500	10.50	0.20
PKS0237–233	2.042163	< 13.300		13.571	0.056	< 13.450	< 14.000	< 12.100	< 11.700	10.10	3.60
PKS0237–233	2.042433	< 12.750		12.618	0.051	< 12.850	< 14.400	< 12.350	< 11.550	11.00	1.00
Q0329–385	2.076432	< 13.700		13.223	0.008	< 12.900	< 13.250	< 11.300	< 11.650	18.10	1.60
Q0329–385	2.352007	< 12.750	< 12.800	13.281	0.011	< 13.350	< 13.800	< 11.850	< 11.550	12.10	0.70
Q0329–385	2.352122	< 13.000	< 12.950	13.103	0.014	< 13.300	< 14.000	< 11.900	< 11.600	41.70	27.00
HE1122–1648	2.030096	< 12.300		12.270	0.041	< 12.950	< 13.900	< 19.900	< 11.400	6.30	1.70
HE1347–2457	2.116199	< 14.100		13.351	0.008	< 12.850	< 15.100	< 11.050	< 11.150	7.70	0.30
HE2347–4342	2.119806	< 14.100		13.286	0.027	< 12.600	< 18.100	< 11.400	< 11.650	7.60	0.20
HE2347–4342	2.274151	< 13.100	< 12.800	13.082	0.070	< 12.850	< 14.000	< 11.500	< 12.100	7.60	0.20
HE2347–4342	2.274295	< 13.500	< 13.700	13.368	0.035	< 12.650	< 14.000	< 11.400	< 12.200	5.40	0.10
HE2347–4342	2.274836	< 13.100	< 19.900	12.607	0.045	< 12.700	< 16.300	< 11.550	< 11.300	25.10	3.10
HE2347–4342	2.274931	< 13.400	< 14.900	12.775	0.128	< 13.000	< 15.300	< 11.900	< 11.650	9.50	1.00
HE2347–4342	2.275343	< 13.300	< 14.900	13.085	0.018	< 12.850	< 14.900	< 11.150	< 11.600	9.40	2.90
HE2347–4342	2.275833	< 12.700	< 12.700	12.486	0.024	< 12.300	< 13.400	< 11.050	< 12.950	6.60	0.80
HE2347–4342	2.276343	< 13.050	< 12.700	12.778	0.010	< 12.250	< 13.300	< 11.650	< 13.700	14.40	0.50
PKS2126–158	2.388883	< 13.600		13.035	0.004	< 17.300	< 13.300	< 11.700	< 12.400	9.80	0.20
PKS2126–158	2.393862	< 14.400		13.633	0.086	< 13.200	< 13.400	< 15.300	< 13.150	5.70	2.40
PKS2126–158	2.394003	< 14.400		13.776	0.075	< 13.300	< 13.150	< 15.900	< 14.200	6.60	0.10
PKS2126–158	2.395156	< 13.600		12.928	0.013	< 12.150	< 13.700	< 11.900	< 12.000	17.10	3.60
PKS2126–158	2.395333	< 13.350		12.924	0.011	< 12.300	< 14.300	< 11.650	< 11.550	8.10	0.40
PKS2126–158	2.396791	< 12.400		11.786	0.060	< 12.800	< 13.800	< 11.900	< 11.400	24.60	1.30
PKS2126–158	2.678806	< 13.700	< 13.250	13.705	0.077	< 13.400	< 14.000	< 13.600	< 13.000	9.90	0.60
PKS2126–158	2.678957	< 14.100	< 14.000	13.852	0.060	< 13.500	< 15.100	< 14.700	< 12.750	26.00	4.50

**Table 4.** High-metallicity component properties

QSO	$z$	$\log n_{\text{H}}$ ( $\text{cm}^{-3}$ )	$\log n_{\text{H}}$ ( $\text{cm}^{-3}$ )	$\log R$ (pc)	[C/H]	$\log f_g$	[Si/C]
(1)	(2)	(3)	(4)	(5)	(6)	(7)	(8)
Q0122–380	2.062560	> -4.22		< 3.17	> -0.34	< -3.49	< 1.80
HE0151–4326	2.415724	> -3.62	< -2.96	< 2.33	> -0.51	< -4.58	< 0.10
HE0151–4326	2.419671	> -3.86	< -3.07	< 2.34	> -0.36	< -4.79	< 0.83
HE0151–4326	2.468097	> -4.25	< -3.44	< 3.04	> -0.07	< -3.80	< 1.13
HE0151–4326	2.468720	> -4.52	< -2.56	< 3.77	> -0.83	< -2.60	< 2.26
PKS0237–233	2.042163	> -4.08		< 3.13	> 0.04	< -3.42	< 0.50
PKS0237–233	2.042433	> -4.92		< 4.27	> -0.36	< -2.00	< 3.45
Q0329–385	2.076432	> -3.81		< 3.00	> -0.62	< -3.42	< 0.33
Q0329–385	2.352007	> -4.11	< -3.60	< 2.64	> 0.34	< -4.44	< 0.67
Q0329–385	2.352122	> -4.37	< -3.27	< 3.42	> -0.09	< -3.15	< 1.46
HE1122–1648	2.030096	> -5.07		< 4.12	> -0.25	< -2.45	< 4.17
HE1347–2457	2.116199	> -3.81		< 3.39	> -0.89	< -2.64	< -0.31
HE2347–4342	2.119806	> -3.64		< 3.06	> -0.89	< -3.14	< 0.03
HE2347–4342	2.274151	> -4.18	< -3.34	< 3.15	> -0.27	< -3.50	< 1.58
HE2347–4342	2.274295	> -3.61	< -2.78	< 2.41	> -0.20	< -4.41	< 0.47
HE2347–4342	2.274836	> -4.64	< 1.67	< 4.07	> -0.72	< -2.13	< 2.36
HE2347–4342	2.274931	> -5.07	< -1.33	< 5.21	> -0.93	< -0.26	< 3.91
HE2347–4342	2.275343	> -4.12	< -1.60	< 3.21	> -0.41	< -3.31	< 0.94
HE2347–4342	2.275833	> -4.18	< -2.90	< 2.75	> -0.42	< -4.30	< 3.02
HE2347–4342	2.276343	> -3.78	< -3.20	< 2.29	> -0.40	< -4.81	< 2.78
PKS2126–158	2.388883	> -3.95		< 3.17	> -0.74	< -3.22	< 1.48
PKS2126–158	2.393862	> -3.71		< 3.50	> -0.92	< -2.33	< 1.31
PKS2126–158	2.394003	> -3.48		< 3.04	> -0.62	< -3.02	< 1.92
PKS2126–158	2.395156	> -3.53		< 2.35	> -0.66	< -4.45	< 0.60
PKS2126–158	2.395333	> -3.68		< 2.40	> -0.51	< -4.50	< 0.35
PKS2126–158	2.396791	> -5.58		< 5.23	> -0.85	< -0.73	< 6.74
PKS2126–158	2.678806	> -4.01	< -3.51	< 3.39	> -0.25	< -2.84	< 1.54
PKS2126–158	2.678957	> -4.03	< -2.93	< 3.83	> -0.49	< -1.98	< 1.16